UNIVERSITY OF COPENHAGEN
FACULTY OF SCIENCE

Master Thesis

Samuel Stokholm Baxter

The Search for Right Handed Neutrinos using the SHiP Experiment

Supervisor: Dr. Stefania Xella

29/08/2016

Abstract

SHiP [1] is an experiment in the planning phase that will search for hidden particles in a high intesity environment.
In this report, the focus will be on the searh for right handed neutrinos (HNLs). The theory motivating this search will be explained, along with some overall details on the planned experimental setup.
I will explore cut based - and multivariate selection. I will also explore the possibility to use particle identification to improve the signal/background ratio for the experiment.
In the end, the sensitivity of the SHiP experiment will be estimated based on the cuts found with particle identification.

Acknowledgments

Thanks are due to the SHiP Collaboration, especially: Thomas Ruf, Elena Graverini, Behzad Hosseini and Nicola Serra, for providing support, feedback and suggestions for the research. Thanks are also due to Oleg Ruchayskyi for theoretical discussions, and to Stavros Kitsios for introducing me to some of the software used in the research.

Contents

Introduction **1**

1 Theory **2**
1.1 The Standard Model . . . 2
1.1.1 Conserved quantities . . . 3
1.1.2 Charge-Parity . . . 4
1.1.3 Shortcomings of the Standard Model . . . 5
1.2 Neutrino Oscillations . . . 6
1.3 The seesaw mechanism . . . 8
1.4 The Neutrino Minimal Standard Model . . . 12

2 The Ship Experiment **16**
2.1 SHiP Detector . . . 16
2.2 SHiP experimental setup . . . 21
2.3 Other Searches with SHiP . . . 24
2.4 Ship Software . . . 25

3 Analysis **27**
3.1 HNL Signal . . . 27
3.2 Neutrino Background . . . 33
3.3 Muon Background . . . 34
3.4 Selection Cuts . . . 35
3.5 Cuts proposed by the SHiP Collaboration . . . 38
3.6 Application of Cuts to HNL Signal and Neutrino Background . . . 40
3.7 Methods for Multivariate Analysis . . . 44
3.7.1 Cuts . . . 44
3.7.2 Likelihood . . . 45
3.7.3 Boosted Decision Tree . . . 47
3.7.4 Evaluation of TMVA methods . . . 49
3.8 Particle Identification . . . 52
3.8.1 Pid Performance . . . 52
3.8.2 Optimisation using Pid . . . 54
3.9 SHiP Sensitivity Range . . . 57

Conclusion **61**

References **62**

Appendix **64**

List of Figures

1 Table of the Standard Model particles 2
2 Arrangements of the neutrino masses with normal hierarchy(left) and inverted hierarchy(right) from [7]. The colours represent the neutrino flavours; e (red), μ (blue) and τ (blue) 7
3 Thermal history of the early universe from [3] 13
4 Constraints on the νMSM from experimental exclusions and theoretical bounds [13]. 14
5 The fermions of the νMSM from [5] 14
6 Arrangement of the straws (left) and a front view the planes in one tracking station (right) from [8] 17
7 Setup of the tracking stations in SHiP as a diagram with magnetic field strength and distance along the Z axis (left) and as a 3d figure (right) from [8] 17
8 a. display model of an Ecal cell, b. 3d model of an Ecal cell, c. 3d model of the Ecal, Hcal and muon stations with the top right quarter removed, from [8] 19
9 The detector segment of the SHiP vacuum vessel. 20
10 Neutrino target and muon magnetic spectrometer from [8] 22
11 Resistive plate chamber [8] 22
12 Sketch of the vacuum vessel of the SHiP experiment, with emphasis on the veto taggers. 23
13 Feynmann diagram for the decay process of a Ds^+ meson creating an HNL and the subsequent decay process for the HNL into; $\pi^+ + \mu^-$ (a), and $\bar{\nu_\mu} + \nu_\mu + \nu_\mu$ (b) 27
14 Distribution of neutrino polar angle from MC simulation 33
15 Distribution of selected variables for the $\pi + \mu$ final state of the HNL and the neutrino background at the reconstruction 36
16 Distribution of selected variables for mixed final state of the HNL and the anti-neutrino background at the reconstruction 37
17 Distributions of variables for mixed HNL signal at 1GeV from TMVA 45
18 Likelihood distribution for signal and background - the filled histogram is the test sample while the errorbar plot is for the training sample 46
19 Optimisation of likelihood cut 46
20 47
21 Boosted decision tree distribution for signal and background - the filled histogram is the test sample while the errorbar plot is for the training sample with mixed HNL signal 48
22 Boosted decision tree cut optimisation for mixed HNL signal . . 48
23 50
24 Branching ratios for the HNL decay modes that are included in FairShip so far as a function of HNL mass with $U^2 = (4.47 \cdot 10^{-10}, 7.15 \cdot 10^{-9}, 1.88 \cdot 10^{-9})$ the dashed lines represent invisible decay modes, while dots show oscillating decay modes. Other decay modes have also been part of the computation of the branching ratios. 58

25 Branching ratios for the HNL decay modes that are not included in FairShip so far as a function of HNL mass with $U^2 = (4.47 \cdot 10^{-10}, 7.15 \cdot 10^{-9}, 1.88 \cdot 10^{-9})$. 59
26 Signal efficiencies for different cuts based on branching ratio . . . 59
27 SHiP sensitivity with background taken into account. 61

List of Tables

1 The fundamental forces in particle physics with the fermions they act on and the gauge bosons that mediate the forces. 3
2 Neutrino mixing parameters for neutrino oscillations from [6] . . 6
3 Branching ratios for the produced charm to the different charmed mesons and the number of produced τ from [5]. 29
4 Branching ratios for the produced charmed mesons to decay into neutrinos that can mix into HNLs. 29
5 Constants used to find the HNL yield 30
6 Values of HNL production rate, lifetime and Lorentz factor in the 1 GeV HNL mass case 31
7 Branching ratios and reconstruction efficiencies for decay modes with an HNL mass of 1 GeV 32
8 Expected HNL yield of the SHiP experiment, given a normal neutrino mass hirarchy with $U^2 = 9.5$ 32
9 Parameters from the HNL with 0.5 GeV mass that are needed to estimate the number of HNLs detected in the ship experiment. . 32
10 Cut efficiencies for HNL decay into $\pi^+ + \mu^-$ 40
11 Cut efficiencies for HNL decay into $\mu^+ + \mu^-$ 40
12 Cut efficiencies for HNL decay into $e + \mu$ 41
13 Cut efficiencies for HNLs with 1 GeV mass decaying into visible final states 41
14 Cut efficiencies for HNLs with 0.5 GeV mass decaying into visible final states 42
15 Neutrino background with cuts applied 42
16 Anti neutrino background with cuts applied 42
17 Using $HNL \to \pi + \mu$ HNL signal with 1 GeV mass 49
18 Using $HNL \to \mu + \mu$ signal with 1 GeV mass 49
19 Using mixed HNL signal with 1 GeV mass 49
20 Cuts from TMVA optimisation on differt types of HNL signal with 1 GeV mass 51
21 HNL signal with 1 GeV mass and all visible decay modes open after the N.d.f cut. The numbers in parenthesis are efficiency/purity 53
22 Neutrino background after the N.d.f cut. The numbers in parenthesis are efficiency/purity 53
23 HNL decay into visible final states with the same cuts applied as in table 13 with the exception of the momentum cut which has been increased to 1.5 GeV 54
24 Neutrino background final states identified with Pid 54
25 HNL final states at 1 GeV according to Pid 55
26 Neutrino final states passing the veto - and fiducial cuts 55
27 Neutrino background after cutting on all variables up to and including Ip$<$250 cm. The numbers in parenthesis are efficiency/purity 56
28 Result from selections with Pid 57
29 Intervals for background level with the required signal to be 3σ away from background 58

Introduction

Neutrinos have some properties that are not explained in the Standard Model [2], so explaining these properties will require modification of the Standard Model. A popular theory to explain the neutrino phenomena is the neutrino minimal extension to the Standard Model (νMSM) [3], that adds a set of right handed neutrinos.
The only interaction these right handed neutrinos undergo is a process called the seesaw mechanism [4], where the right handed neutrinos couple to left handed neutrinos. The consequenses of this seesaw mechanism are that the left handed neutrinos are given a small mass, and that the neutrino flavour oscillations can occur.
These right handed neutrinos can in principle have a mass up to $\sim 10^{15} GeV$ [5], and their mass can even go down to the mass of left handed neutrinos.
This means that the right handed neutrino can either be found in a high energy experiment, assuming a mass at the order of TeV and strong enough coupling to be detected, or in a high intensity experiment, where it is possible to discover particles with a very low copling as long as the mass is low as well, typically a few hundred MeV.
The SHiP experiment is going to look for right handed neutrinos with a mass ranging from 100 MeV to a few GeV in a high intensity environment, where the limiting factor is the right - left handed neutrino mixing parameter U^2.
In this report, I will investigate how to search for right handed neutrinos in SHiP.
I will explore cut based - and multivariate selection. I will also explore the possibility to use particle identification to improve the signal/background ratio of the experiment.
In the end, the sensitivity of the SHiP experiment will be estimated after applying cuts found using particle identification.

1 Theory

In this chapter I will go through some of the theory that motivates the search for right handed neutrinos.

1.1 The Standard Model

In the Standard Model, there are three fundamental forces, which are mediated by exchanging gauge bosons.
There are 12 fermions, which are divided into 2 categories, quarks and leptons as seen in fig. 1. The fermions are also divided into generations, where a set of 2 quarks and 2 leptons belong to each generation. Each column of fermions in fig. 1 represents a generation.

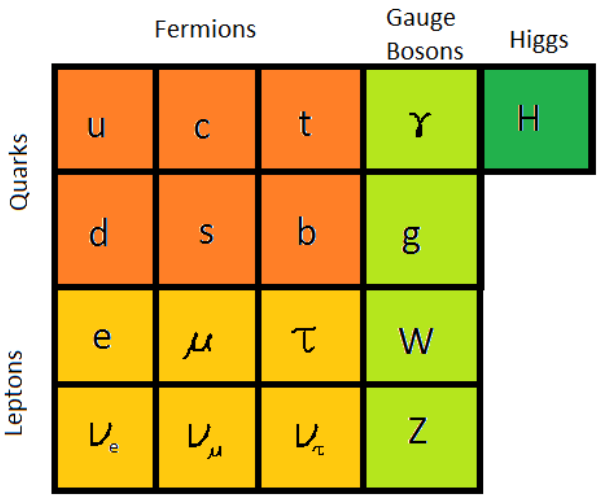

Figure 1: Table of the Standard Model particles

The three forces are the electromagnetic, strong, and weak force.

The electromagnetic force attracts particles of opposite charge and repels particles of the same charge. It is mediated by photons (γ).

The strong force confines quarks in hadrons and is mediated by gluons (g).

Weak interactions are either mediated by W^+ or W^- bosons which is called a charged current interaction or by Z^0 bosons called neutral current interactions. These gauge bosons have a mass of the order of 100 GeV. The large mass of the W and Z bosons leads to the fact that they can only be exchanged over very short distances, which can be approximated to point like interactions at low energies.

One can see a summery of the forces and the particles in table 1

Force	Works on	Mediated by
Strong	quarks	g
Electromagnetic	quarks charged leptons	γ
Weak	quarks charged leptons neutrinos	$W^{\pm}$ Z^0

Table 1: The fundamental forces in particle physics with the fermions they act on and the gauge bosons that mediate the forces.

Most of the processes in particle physics involve relativistic particles. Therefore, one has to describe the phenomena from a relativistic perspective, which means that one wants to work with quantities that are invariant under Lorentz transfomation.
The Standard Model is therefore often formulated by a Lagrangian, where the classical variables $q(t)$ and t are replaced by $\phi(s)$ and $s(\mathbf{x}, t)$. The variable $q(t)$ is the point in space for a given particle at a given time, t is the time, $s(\mathbf{x}, t)$ is a point in space-time, and $\phi(s)$ is the field at a given point in space-time.

One important property of particles undergoing weak interactions is whether the particle is left - or right handed.
A particle is right handed if its spin points in the direction of its momentum, while it is left handed if its spin points in the opposite direction of its momentum.
The property of being left - or right handed is called chirality.
For a massles particle, chirality is invariant under Lorentz transformation, while it can be reversed for a massive particle.
A right handed neutrino does not exist in the Standard Model, therefore the neutrino has to be massless according to the Standard Model.

In the Standard Model the obseved masses are attributed to a coupling to the Higgs field.

1.1.1 Conserved quantities

In the Standard Model, certain properties are expected to be conserved in certain processes, so in general violations are sought for in order to discover new physics.
Lepton number is one property that is required to be conserved in the Standard Model, but violation of this number is already discovered through neutrino oscillations.
Lepton number violation is also a key feature of the νMSM.

Lepton number is the number of leptons (including neutrinos) of a certain genaration minus the number of anti-leptons of a particular flavour.
So if for example a neutron decays into a proton and an electron, the decay

must also include an anti-electronneutrino in order to be a valid process since the electron number for a neutron is zero.

If the lepton number proves to be violated, one can require the of conservation of the total lepton number instead.
The total lepton number is the sum of lepton numbers for each flavour.

Even though neutrino oscillations do not conserve lepton number, the total lepton number is still conserved.
Any violation of lepton number observed in experiments will force us to extend the Standard Model with a lepton number violating process or invent a completely new theory.

Interaction processes are required to follow the principle of baryon number conservation, that for processes creating new baryons it must also create an equal number of antibaryons. The baryon number is defined by the following equation: $B = [N(q) - N(\bar{q})]/3$, where $N(q)$ is the number of quarks and $N(\bar{q})$ is the number of antiquarks.

For the strong - and electromagnetic forces it is also required that each quark number is conserved, which means that strong - and electromagnetic forces can only create quark - antiquark pairs of the same flavour.

Weak forces can violate quark number, but not baryon number.

1.1.2 Charge-Parity

Parity is inverting the sign on the spatial coordinates and is conserved(meaning invariant under parity transformation of the interaction process) in strong and lectromagnetic interactions, but not in weak interactions.

In spherical coordinates, parity transformation corresponds to $r \to r$, $\theta \to \pi - \theta$ and $\phi \to \pi + \phi$. Under parity transformation, momentum is reversed but angular momentum and spin remains the same. This means that chirality is reversed, for example a left handed particle turns into a right handed particle.

The charged current interaction works on leptons that are left handed and their right handed antiparticles. The neutral current interaction can also involve right handed charged leptons, but not right handed neutrinos.

Since these weak processes are not invariant if the chirality is reversed, they are not invariant under parity transformation.

When multiplying with the charge conjugation however, the weak interactions involving leptons conserve this quantity (charge-parity or CP). By charge conjugation is understood changing a particle into its corresponding anti particle. Just like parity, charge conjugation is conserved with strong - and electromagnetic processes but is violated in weak interactions. This is because if a left handed particle is charge conjugated, it will be a left handed anti-particle,

which does not interact in certain weak processes. When one uses a parity transformation and charge conjugation, a left handed particle becomes a right handed anti-particle. Since both left handed particles and right handed anti-particles are allowed in weak interactions, the weak process is invariant under the combined charge-parity transformation. This is usually abbreviated to CP conservation.

Most particles require only charge conjugation to become their anti-particles, but the neutrino requires both charge conjugation and parity transformation. There are still some violations of CP observed, which result in the inclusion of CP violating phases to account for these observed anomalies.

1.1.3 Shortcomings of the Standard Model

Even though the Standard Model generally makes accurate predictions of particle phenomena, yet there are still some observed phenomena that are not accounted for in the Standard Model.

These shortcomings are listed below:

Dark matter [3] - The Standard Model does not contain particles that are heavy and abundant enough to be the astronomically observed dark matter.

Neutrino oscillations [3] - A requirement for neutrino flavour oscillations is that neutrinos have mass, which they don't in the standarsd model, furthermore a neutrino oscillation is a lepton flavour violating process which is not allowed in the Standard Model.

Baryon asymmetry of the early universe [3] - The processes included in the Standard Model do not explain a symmetry breaking of matter vs antimatter anywhere close to what is expected in the early universe right after the big bang.

Present accelerated expansion of the universe [3] and inflation in the early universe - these phenomena cannot be explained with the Standard Model.

There are many hypotheses explaining these phenomena by introducing new particles and other parameters. The challenge is to put these hypotheses to the test by searching for the particles used in a given hypothesis.

1.2 Neutrino Oscillations

One observed and well documented feature of the neutrinos is their ability to change flavour over great distances. In order for that to happen, neutrinos need to have some mass and some mass eigenstates that are linear combinations of the flavour eigenstates, so that the mass eigenstate can mix back to a different flavour eigenstate than it originally was.

The relation between the mass - and flavour eigenstates of the neutrinos is described below:

$$\begin{pmatrix} \nu_e \\ \nu_\mu \\ \nu_\tau \end{pmatrix} = V_{PMNS}(\theta_{12}, \theta_{13}, \theta_{23}, \delta, \alpha_1, \alpha_2) \begin{pmatrix} \nu_1 \\ \nu_2 \\ \nu_3 \end{pmatrix} \text{[6]}, \tag{1}$$

where θ_{12}, θ_{23}, θ_{13} are the mixing angles between the flavour - and mass eigenstates of the neutrinos, δ is the Dirac CP violating phase, α_1 and α_2 are the Majorana CP violating phases of the active neutrinos. The experimental values for these parameters are shown in table 2, except for α_1 and α_2 since these parameters are still unkown.
Representative values for these parameters are given for normal neutrino mass hierarchy in table 2.

$\sin^2\theta_{12}$	0.308 ± 0.017
$\sin^2\theta_{23}$	$0.437^{+0.033}_{-0.023}$
$\sin^2\theta_{13}$	$0.0234^{+0.0020}_{-0.0019}$
δ/π	$1.39^{+0.38}_{-0.27}$

Table 2: Neutrino mixing parameters for neutrino oscillations from [6]

The PMNS matrix can then be written as follows:

$$V = \begin{pmatrix} c_{12}c_{13} & s_{12}c_{13} & s_{13}e^{-i\delta} \\ -s_{12}c_{23} - c_{12}s_{23}s_{13}e^{i\delta} & c_{12}c_{23} - s_{12}s_{23}s_{13}e^{i\delta} & s_{23}c_{13} \\ s_{12}s_{23} - c_{12}c_{23}s_{13}e^{i\delta} & -c_{12}s_{23} - s_{12}c_{23}s_{13}e^{i\delta} & c_{23}c_{13} \end{pmatrix} \cdot \begin{pmatrix} 1 & 0 & 0 \\ 0 & e^{i\alpha_1/2} & 0 \\ 0 & 0 & e^{i\alpha_2/2} \end{pmatrix} \text{[6]}, \tag{2}$$

where $s_{ij} = \sin(\theta_{ij})$ and $c_{ij} = \cos\theta_{ij}$.

The masses of the neutrinos are given such that m_1 is the mass of ν_1, m_2 is the mass of ν_2 and m_3 is the mass of ν_3.
Based on the observed neutrino oscillations, two mass differences have been found:

$\Delta m^2_{21} \equiv \Delta m^2_\odot = 7.54^{+0.26}_{-0.22} \cdot 10^{-5} eV^2$[6], which is obtained from solar neutrino oscillations.

$\Delta m^2_{31} \equiv \Delta m^2_{atm} \approx 2.43 \pm 0.06 \cdot 10^{-3} eV^2$[6], which is obtained from atmospheric neutrino oscillations.

These values are given for normal neutrino mass hierarchy.
It is still unknown which of the neutrino mass eigenstates is the lightest, along with what the mass of the lightest neutrino is. Only the relation between m_1 and m_2 has been determined in order to conclude that $m_2 > m_1$ by finding $\Delta m^2_{\odot}$ to be positive. One has not yet found the sign on Δm^2_{atm}, so there are two models for neutrino mass hierarchy.

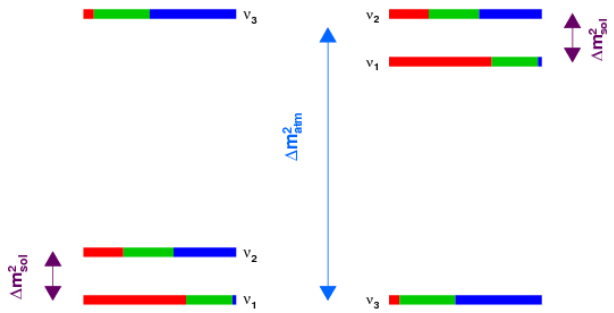

Figure 2: Arrangements of the neutrino masses with normal hierarchy(left) and inverted hierarchy(right) from [7]. The colours represent the neutrino flavours; e (red), μ (blue) and τ (blue)

The two models for neutrino mass hierachy are called normal hierachy and inverted hierachy, and one can see a visualisation of the squared mass differences of the two models in fig. 2.

Normal hierachy puts the neutrino masses in the following order,
$m_1 < m_2 < m_3$ with the following mass differences:

$$\Delta m_{21} = \sqrt{\Delta m^2_{\odot}} = 8.68 \pm 0.13 \cdot 10^{-3} eV$$

$$\Delta m_{31} = \sqrt{\Delta m^2_{atm}} = 4.93 \pm 0.06 \cdot 10^{-2} eV$$

Inverted hierachy puts the neutrino masses in an alternative order,
$m_2 > m_1 > m_3$ with the mass diferences:

$$\Delta m_{13} = \sqrt{\Delta m^2_{atm} - \Delta m^2_{\odot}} = 4.85 \pm 0.06 \cdot 10^{-2} eV$$

$$\Delta m_{23} = \sqrt{\Delta m^2_{atm}} = 4.93 \pm 0.06 \cdot 10^{-2} eV,$$

1.3 The seesaw mechanism

There are many things that are still unknown about neutrinos - among these the question whether neutrinos are Dirac - or Majorana particles. All neutrinos are left handed while all anti-neutrinos are right handed according to experiments and the Standard Model.

The previously mentioned neutrino oscillations require that at least three mass eigenstates exist, where at least two of them have nonzero mass.
Since the existence of right handed neutrinos is denied in the Standard Model, left handed neutrinos can not couple to the Higgs with a Yukawa coupling like the rest of the fermions can. [9]

One could make an alternative coupling to the Higgs, but then one would either have to sacrifice renormalizability of the Standard Model or invent a new Higgs. [9]
Even if one uses one of these ways to give mass to left handed neutrinos, the mass is still of the order 10^{-5} compared to the u quark [4].

The neutrino masses can be explained when including a set of leptons, N_I where $I = \{1, 2, ..., \mathcal{N}\}$ that are neutral and right handed. They are therefore called right handed neutrinos. Doing so is going beyond the standard model and lepton number violation is a possibility. [4]

Since right handed neutrinos are not involved in any interactions, they have no charges that need to be conserved. This means that they can have mass without coupling to the Higgs, a so called Majorana mass.

With the introduction of right handed neutrinos, coupling to the Higgs is now possible for left handed neutrinos resulting in a Dirac mass.

This means that one can extend the Lagrangian for the Standard Model ($\mathcal{L}_{\text{SM}}$) with the properties made possible by adding N_I with terms for kinetic energy, left - right handed neutrino coupling to the Higgs, and Majorana mass for the right handed neutrinos.

The extended Lagrangian is seen below:

$$\mathcal{L} = \mathcal{L}_{\text{SM}} + i\bar{N}_I\gamma^\mu\partial_\mu N_I - \left(F_{\alpha I}\bar{L}_\alpha N_I\tilde{\Phi} + \frac{M_{I,J}}{2}\bar{N}_J^C N_I + h.c.\right), \tag{3}$$

[10] where $\mathcal{L}_{\text{SM}}$ is the Lagrangian for the Standard Model, L is the left handed lepton doublet with $L_\alpha = \begin{pmatrix}\nu_\alpha \\ \alpha\end{pmatrix}$ where $\alpha = \{e, \mu, \tau\}$, $\tilde{\Phi}$ is the Higgs doublet with a vacuum expectation value of $\tilde{\Phi} = \frac{1}{\sqrt{2}}\begin{pmatrix}v \\ 0\end{pmatrix}$ [5], and$F$ is the Yukawa coupling between the left - and right handed neutrinos. One can see further details on this Lagrangian in the appendix.

In the following, a scenario where both left - and right handed neutrinos are Majorana particles is described, meaning that their effective masses are Majo-

rana masses.
This means that the right handed neutrino is allowed to be much heavier than the left handed neutrino, and one can derive the effective Majorana masses of the left handed neutrinos, which is much smaller than the Dirac mass.

The effective Lagrangian for masses can be written in matrix form as follows, where L has been replaced by ν, going from lepton doublets to only left handed neutrinos:

$$\mathcal{L}_{mass} = -\frac{1}{2}(\bar{\nu}\bar{N}^c)\mathcal{M}_{\nu,N}\begin{pmatrix}[4]\nu^c\\ N\end{pmatrix} + h.c. \tag{4}$$

where

$$\mathcal{M}_{\nu,N} = \begin{pmatrix}\underline{0} & m_D\\ m_D^T & M_N\end{pmatrix}[4], \tag{5}$$

where $\underline{0}$ is an empty Majorana mass matrix, which comes from the fact that left handed neutrinos are massles in the Standard Model.
The Dirac mass matrix, m_D is a $3\times\mathcal{N}$ matrix where each matrix element follows the relation:

$$(m_D)_{\alpha,I} = F_{\alpha,I}\cdot v,$$

where $v = \sqrt{2}\langle\Phi\rangle \approx 246GeV$ [6] where Φ is the Higgs field.
$F_{\alpha,I}$ is the Yukawa coupling between the left - and right handed neutrinos.
M_N is the $\mathcal{N}\times\mathcal{N}$ Majorana mass matrix. For simplicity, one can assume this matrix to be diagonal.
The mixing angle, Θ between left - and right handed neutrinos relates to the Dirac mass matrix as follows:

$$\Theta \equiv -m_D\cdot M_N^{-1}[3]$$

One can then define $U_\alpha^2 \equiv \sum_{I=1}^{\mathcal{N}}\Theta_{\alpha,I}\Theta_{\alpha,I}^*$ [3].
Furthermore, one can define $U^2 \equiv \sum_\alpha U_\alpha^2 = Tr(\Theta^\dagger\Theta)$ [3].
These values are the relevant parameters for a direct search experiment [3].

In the limit where $m_D \ll M_N$, one can find the eigenvalues of $\mathcal{M}_{\nu,N}$ to obtain the masses for the mass eigenstates of both left - and right handed neutrinos.

Let's start with the simplest case, where we have 1 left handed neutrino state and 1 right handed neutrino state, then one has a 2×2 matrix where m_D, M_N and $\underline{0}$ each have a single value.
One can then find the eigenvalue λ by solving:

$$\det(\mathcal{M}_{\nu,N} - \lambda\cdot\underline{I}) = 0$$

where $\underline{I}$ is the identity matrix.

This results in the polynomial; $\lambda^2 - \lambda M_N - m_D^2 = 0$ with the solution:

$$\lambda = \frac{M_N \pm \sqrt{M_N^2 + 4m_D^2}}{2} = \frac{M_N \pm M_N\sqrt{1 + 4m_D^2/M_N^2}}{2} \approx \frac{M_N \pm M_N(1 + 2m_D^2/M_N^2)}{2}.$$

This means that the mass eigenstate for the left handed neutrino is $M_N + \frac{M_D^2}{M_N}$, which is basically M_N due to the assumption that $m_D \ll M_N$.
The effective mass for the left handed neutrino is then $m_\nu = -\frac{m_D^2}{M_N}$.

If one assumes that $m_\nu = m_{atm} \approx 0.05$eV, where $m_{atm} = \sqrt{\Delta m_{atm}^2}$ is the mass difference obtained from atmospheric neutrino oscillations [6].
When ignoring the sign on the mass eigenvalue, that implies that m_D is complex, one can use the relation $m_D^2/M_N = 0.05$ eV to find fitting candidates for the mass of the right handed neutrino and the Dirac mass term.

It turns out that one can choose any mass for the right handed neutrino as long as $m_\nu \ll M_N$, one just has to scale m_D along with it.
If one chooses $M_N = 1$ GeV , then $m_D = 7.07$ keV and the Yukawa coupling will be $F^2 = m_D^2/v^2 \equiv 8.26 \cdot 10^{-16}$.

The mixing angle squared between left - and right handed neutrinos is: $\Theta^2 = m_D^2/M_N^2 = 5 \cdot 10^{-11}$.

These results can be extended to cover all flavours of left handed neutrinos, and additional right handed neutrinos, where instead of a mass for the left handed neutrino, one obtains a mass matrix, m_ν given below.

$$m_\nu = -m_D M_N^{-1} m_D^T [3] \tag{6}$$

This matrix contains elements of the form $(m_\nu)_{\alpha,\beta} = -\sum_I^{\mathcal{N}} \frac{(m_D)_\alpha (m_D)_\beta}{M_I}$, where α and β are indexes for left handed neutrino flavour.
It should be noted that m_ν is an approximate result in the limit $\det(m_D) \ll \det(M_N)$ obtained by block diagonalisation [3].

The matrix m_ν is not neccessarily diagonal, but since it is symmetric it can be diagonalized in order to find the mass eigenvalues as follows:

$$V^T m_\nu V = \mathrm{diag}(m_1, m_2, m_3) [10] \tag{7}$$

Since the matrix V is used to diagonalize the mass matrix m_ν, it must be the same matrix that transforms the neutrino flavour basis into the neutrino mass basis, which is the PMNS matrix in eq. 2.

One can also apply the PMNS matrix to m_D instead, which means that one is shifting from the flavour basis to the mass basis for the left handed neutrinos before applying the seesaw, resulting in the diagonalized version of m_ν. The transformed Dirac mass matrix takes the form: $\tilde{m}_D = V^T \cdot m_D$ [10].

An example is given in [10], where $\mathcal{N} = 3$ and N_1 is taken to be massless with no Yukawa coupling to the left handed neutrinos. N_2 and N_3 are then the effective right handed neutrinos in the seesaw mechanism. This example is

very close to the νMSM, where the first right handed neutrino is a dark matter candidate with a negligible Yukawa coupling and a negligible mass.

The interesting parameter to determine in this model is U^2, since a direct search for the right handed neutrino is limited by this parameter.
The transformed Dirac matrix is written in terms of the effective masses for left handed neutrinos in [10], that can be directly compared to the masses of the left handed neutrinos determined by experimental results.

The mixing angle between active - and sterile neutrinos is defined as:

$$U_\alpha^2 \equiv \sum_I^{\mathcal{N}} |(m_D M_N^{-1})_{\alpha,I}|^2 [10].$$

In order to find U^2, one has to use the PMNS matrix to transform $\tilde{m}_D$ into m_D with the relation $m_D = V^* \tilde{m}_D$.

Assuming that the Yukawa coupling summed over left handed neutrino flavour indices is the same for N_2 and N_3, one obtains the following:

$$U_\alpha^2 = \frac{1}{M}(|V_{\alpha 3}|^2 m_3 + |V_{\alpha 2}|^2 m_2)[10] \tag{8}$$

One thing that is important to notice is the fact that the PMNS matrix is unitary, meaning that the sum of the elements in a row or column multiplied by their complex conjugate add up to 1.
This means that $\sum_\alpha |V_{\alpha 3}|^2 = \sum_\alpha |V_{\alpha 2}|^2 = 1$ and one ends up with:

$$U^2 = \frac{1}{M}(m_3 + m_2)$$

This value is fixed for a given mass and is considered the lower bound on U^2 from the seesaw mechanism.

1.4 The Neutrino Minimal Standard Model

An interesting theory has been introduced involving three right handed neutrinos, one with a keV mass scale (N_1) and two with GeV mass scale (N_2, N_3) and is called the neutrino minimal Standard Model (νMSM). This theory not only explains neutrino mass and - oscillations, but also how matter was generated in the early universe. In addition, it comes with a dark matter candidate in the form of one of the right handed neutrinos.
The dark matter candidate is N_1, that either has no coupling to the active neutrinos or a negligible one compared to N_2 and N_3 in order for it to have a lifetime longer than the age of the universe. N_2 and N_3 are there to account for the two mass differences measured for left handed neutrinos and are the key components for the seesaw model explained above.

A key feature of the of the νMSM is to explain the cosmological phenomenon of baryon asymmetry in the early universe.

The universe has a baryon density normalized to entropy can be found as $n_b/n_\gamma = \Omega_b h^2 \cdot 273.9 \cdot 10^{-10}$ [3], and using $s = 7n_\gamma$ [5] along with $\Omega_b h^2 = 0.02207$ [11], one obtains the result $n_b/s = 8.64 \pm 0.12 \cdot 10^{-11}$.

This also puts a minimum limit on the generation of baryon asymmetry in the early universe, that a good extension to the Standard Model has to account for.
The conditions for this baryon asymmetry are given as follows:

Baryon number violation [5].
In order to increase the baryon number, there must be some process that violates this number.

C and CP violation [5].
The baryon number violating process cannot generate baryon asymmetry if it works for both baryons and antibayons.

Departure from thermal equilibrium [5]
If the process violating baryon number (or any other quantum number) happens at thermal equilibrium, the effect is washed out.

Right handed neutrinos in the GeV mass range can cause this asymmetry by oscillating between types of right handed neutrinos resulting in a lepton asymmetry. One can see the sequence of events in the early universe in the νMSM that leads to baryon asymmetry of the early universe and dark matter production in fig 3.

This phenomenon occurs in the limit: $M_N \ll T_W$, where T_W is the sphaleron freeze out temperature at $\sim 140 GeV$ [3]. For this baryon asymmetry to occur, oscillations of the right handed neutrinos are required. This means that the assumption of the M_N being diagonal is not correct, therefore a free parameter arises from the ratio of the Yukawa couplings to each right handed neutrino [12]. This means that U^2 can assume any value under the condition that baryon

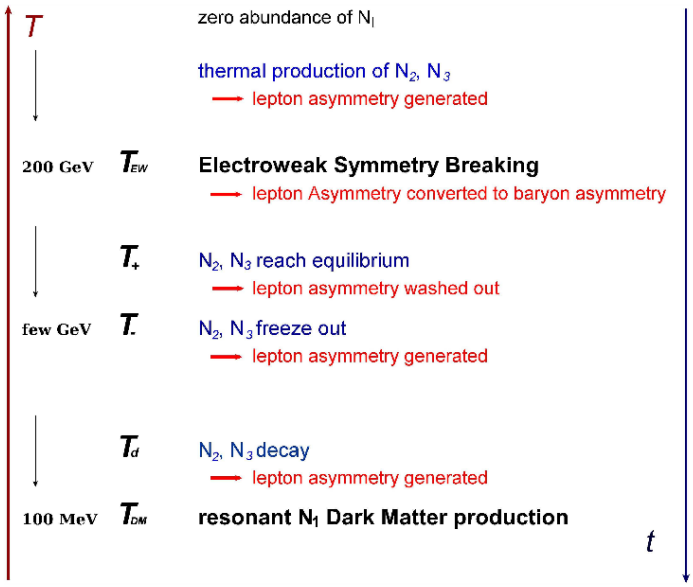

Figure 3: Thermal history of the early universe from [3]

asymmetry of the early universe is generated.

One obtains the upper limit for U^2;
$U^2 < 2.5 \cdot 10^{-7}(GeV/M_N)^{3/2}$ [13] for normal hierarchy.
If U^2 is above this value, it will not be possible to generate the required asymmetry of the universe with the exact conditions from the νMSM [3]. If a right handed neutrino is observed above this limit, one would have to make adjustments in order to explain the baryon asymmetry of the early universe. There is also a lower limit on U^2, but it is lower than other constraints.

While the νMSM is supposed to cause baryon asymmetry in the early universe, it is not supposed to interfere in the nucleosynthesis after the big bang, which gives a constraint on the lifetime of the right handed neutrino, $\tau_N < 0.1s$.[3]
The last constraint on the νMSM comes from the seesaw mechanism derived in section 1.3, so $U^2 \geq 5.8 \cdot 10^{-11}(GeV/M_N)$.

One can see the theoretical constraints along with experimental exclusion regions in fig. 4.

The right handed neutrinos in this model are also called heavy neutral leptons(HNLs), since the right handed neutrinos are much heavier than left handed neutrinos.
The theory also completes the Standard Model in the sense that there is a right handed neutrino for each flavour of neutrinos, just like for the rest of the fermions as displayed in fig. 5.

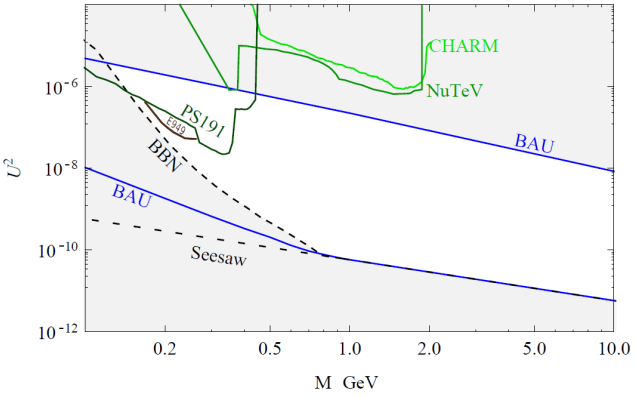

Figure 4: Constraints on the νMSM from experimental exclusions and theoretical bounds [13].

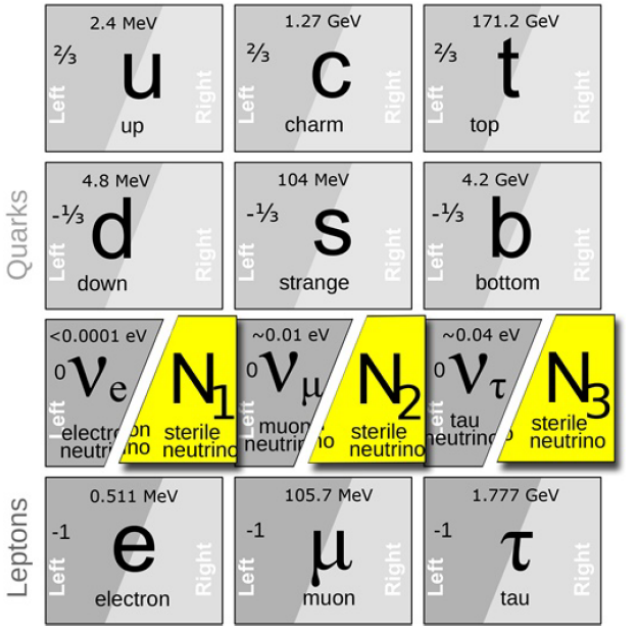

Figure 5: The fermions of the νMSM from [5]

The parameter space for HNLs is usually given as U^2 vs HNL mass. There are some constraints, like the mass difference between N_2 and N_3, which has a maximimum value of $\mathcal{O}(keV)$ [3]. This result means that N_2 and N_3 are practically degenerate.

This potential extension to the Standard Model is very appealing due to the many phenomena it can explain in a relatively simple way.
Therefore, a group of experimentalist at CERN [14] has taken up this theory and proposed a new experiment, SHiP to see if one can find one of the right handed neutrinos in a direct search.

2 The Ship Experiment

This Chapter covers the expected experimental setup along with the software used in this project.

2.1 SHiP Detector

In order to understand the experimental setup for SHiP, I will explain some basics about the types of detectors planned to be used in SHiP.

Tracks from charged particles, that could originate from an HNL decay, are detected by straw trackers.

Straw trackers consist of several gas filled straw tubes. Each tube has a very thin wire inside. An electric potential is set between the wire and the wall of the tube. The wire will be positively charged (anode) so the electrons will drift towards it, while the wall is negatively charged (cathode) at least relative to the wire.

It measures first the passing of the charged particle after which the gas inside the straw will be ionized at the location where the particle went through. The free electrons then drift towards the anode wire, while the ions drift towards the cathode wall. Using the time between the passing of the particle and the drift time for the electrons, one can find the location of the particle.

The straws are assembled in planes with 2 layers of straws as seen in fig. 6.

A straw tracker only carries information about the position perpendicular to the straw, while the position along the straw can not be determined by a single straw. One works around this problem by having series of straw planes where some planes are tilted by a few degrees. This tilting is called a stereo angle. Perpendicular orientation of the planes would lead to "ghost hits" if multiple tracks hit the planes simultaniously.

The planes are assembled in tracking stations, where each station has 4 planes of straw trackers, meaning that each station has 8 layers of straw tubes [8].
The planes are arranged in the order; Y-U-V-Y, where Y is horisontal alingnment of the straws and U has a stereo angle of $5°$ while V has a stereo angle of $-5°$ [8]. One can see a front view of this allignment in fig. 6
There are 4 tracking stations, which are part of the SHiP detector [8].

One can measure the momentum of a detected particle when one also uses a bending magnet, using the following equation:

$$\vec{P} = 0.3 \times \vec{B} \times \vec{R}[16], \tag{9}$$

where $\vec{P}$ is the momentum in GeV, $\vec{B}$ is the magnetic field in T and $\vec{R}$ is the radius of the circle from the bending in m.

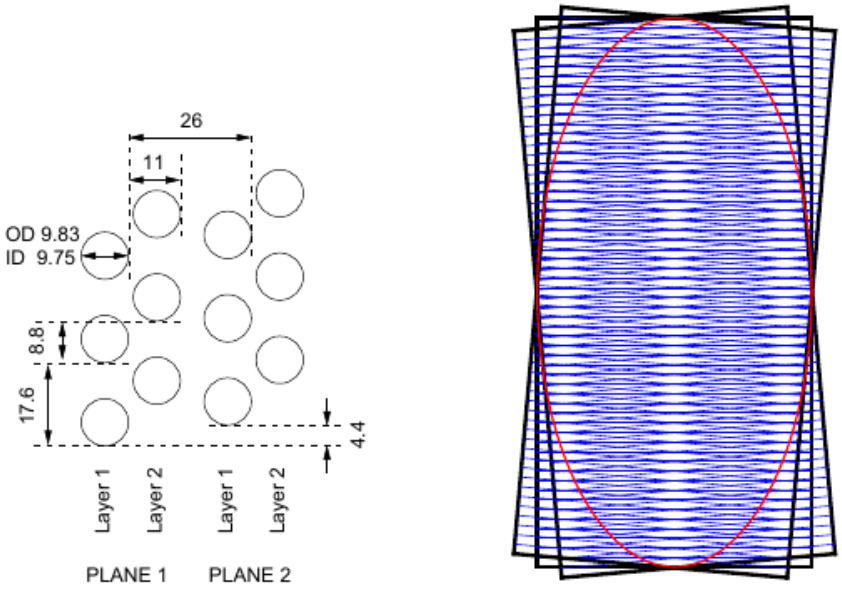

Figure 6: Arrangement of the straws (left) and a front view the planes in one tracking station (right) from [8]

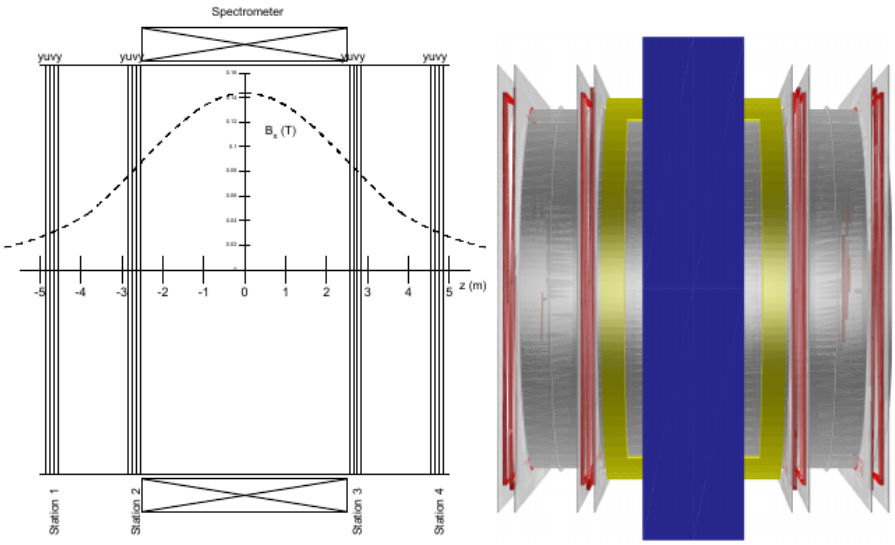

Figure 7: Setup of the tracking stations in SHiP as a diagram with magnetic field strength and distance along the Z axis (left) and as a 3d figure (right) from [8]

A bending magnet is therefore placed between the second and third station in the SHiP detector as displayed in fig. 7.

The bending magnet has a magnetic field strength of up to 0.14 T along the x-axis at the middle between the 2nd and the 3rd tracker station where it peaks. At the 2nd and 3rd tracking station the magnetic field is 0.08 T and a field integral along the z axis between the two stations is ≈ 0.65 Tm [8].

One wants the best spatial resolution on the axis of the bending which is obtained wen aligning the straws perpendicular to the direction of the bending, hence the horisontal orientation of the straws in fig. 6, giving a good resolution on the y-position of a detected particle.

Straw detectors are not sensitive to photons or neutral particles. Straw detectors enable measurement of position and momentum of incoming charged particles and have a low material budget, however this is not enough to identify the particles coming through.

One type of detectors, which is used many places in SHiP is the scintillator. A scintillator consists of a sensitive material that can detect incoming charged particles. The active components are excited to a higher energy level and emit a photon after relaxing to a slightly lower energy level in order to be self transparent. Scintillators are excellent at detecting incoming charged particles. The drawbacks with scintillators are that the spatial resolution is insufficient for tracking purposes.

For particle identification purposes the SHiP experiment is fitted with an electromagnetic calorimeter (Ecal), a hadronic calorimeter (Hcal) and muon stations.

One uses calorimeters to find the energy of particles that can be stopped with reasonable amounts of material. When the particle is stopped, it releases its energy, which is then detected. A general way to achieve this is to shift between a layer of high density material and scintillator. The high density material is there to stop the incoming particle, while the scintillator is there to detect the emitted radiation from the stopping process.

The energy of electrons and photons is measured by using an electromagnetic calorimeter.
The energy deposition happens when an incoming electron emits bremsstrahlung photons in the absorbing materal, which then form electron positron pairs. This cascade of electrons and positrons is detected by the scintillating material and one can use a relation between the number of generated particles and the energy of the incoming particle. The depth at which the shower is most intense is related to the energy of the incoming particle as follows:

$$t_{max} = \log(\frac{E}{E_c})[16], \tag{10}$$

where t_{max} is the depth, in units of the radiation length X_0, where the density of electrons and positrons is highest, E is the particle energy, E_c is the critical

energy which depends on Z, the atomic number of the absorbing material.

The Ecal used in SHiP consists of layers of lead and scintillator [8], the Ecal will be 43.88 cm thick whereof 14 cm is lead that is divided into 140 plates with a thickness of 1 mm each [8], between each lead plate there is a 2 mm scintillator plate [8]. The Ecal is divided into 6×6 cm^2 cells [8] as seen in fig. 8a.

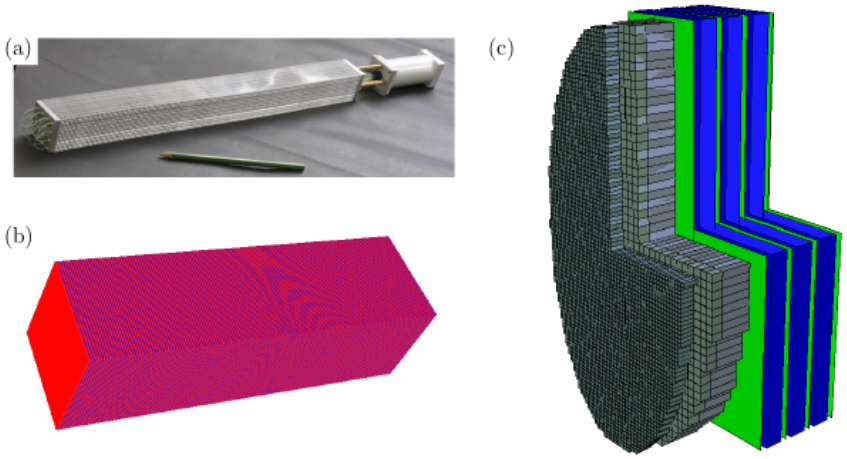

Figure 8: a. display model of an Ecal cell, b. 3d model of an Ecal cell, c. 3d model of the Ecal, Hcal and muon stations with the top right quarter removed, from [8]

The hadronic calorimiter works after the same principle as the electromagnetic - with the difference that it is larger in order for the hadrons to do inelastic scattering in the materal and start a shower. Since hadrons are heavier than electrons, more material is required to stop them, but because of strong interactions one will be able to stop the hadrons with much less material than is required to stop a muon that has approximately the same mass as pion.

Hadrons are so called minimum ionizing particles until their momentum is down to around the rest mass of the particle, whereafter they will deposit the rest of their energy over a rather short distance forming a "Bragg peak"[16].

This means that there might be some energy deposition from the hadron in the electromagnetic calorimeter, but the vast majority of the energy deposition is in the hadronic calorimeter.

The Hcal in SHiP is set up in a similar manner to the Ecal for simplicity in the simulation with 15 mm iron plates and 5 mm scintillator plates [8]. The plan is to divide the Hcal into 2 sections where one has 18 layers [8], while the other section has 48 layers [8], meaning that the Hcal will have 66 layers in total with 99 cm of iron and 33 cm of scintillator. The total thickness of

the Hcal station will be 232 cm [8]. The Hcal is divided into 24×24 cm^2 cells [8].

The muon stations will consist of plastic scintillator bars, 2 cm thick [8], and the muon stations will be 1 m apart from eac other [8]. Between each muon station there will be an iron wall about 50 cm thick [8].

There is a timing detector between the last straw station and the electromagnetic calorimeter (Ecal). It is required to have a timing resolution of $\sim 100ps$ which can be achieved with scintillators [8] or a multiple resistive plate chamber (MRPC) [8]. This timing detector will enable a significant reduction in combinatorial background in the experiment.

The SHiP detector setup is summarized in fig. 9.

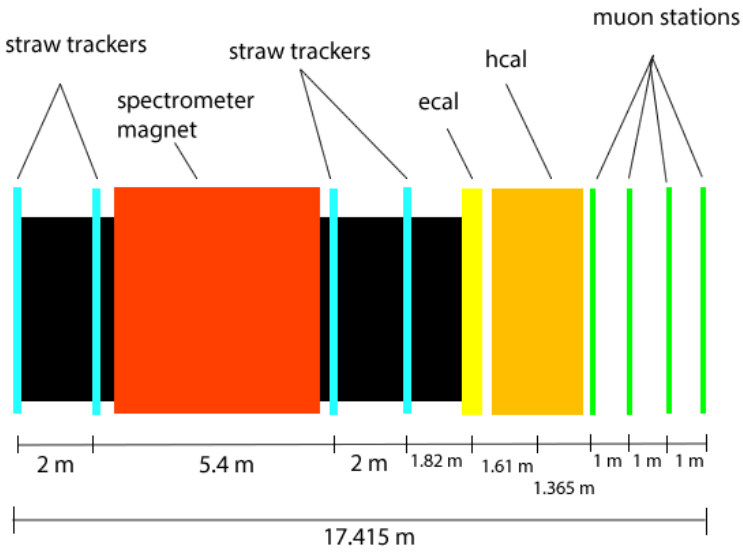

Figure 9: The detector segment of the SHiP vacuum vessel.

2.2 SHiP experimental setup

The experiment will be placed at a beam dump at the SPS at CERN with a 400 GeV proton beam [8].
It is a fixed target experiment, meaning that the centre of mass energy is around 27 GeV [8].
At this limit, one can produce charmed mesons and in addition there will also be a small production of bottomium [8]. This means that it is possible to generate HNLs with a mass up to the mass of bottomium which is about 5 GeV [6].

The target is planned to be a 58 cm Molybdenium block [8] followed by a 58 cm Tungsten block [8] with some water cooling involved as well [8]. The combination of a Molybdenium - and a Tungsten target is chosen in order to maximize the production of heavy hadrons, while minimizing the neutrino - and muon production and containing the rest of the hadron shower [8].
The target will be placed in an iron bunker with a hole upstream of the target for the beam [8]. The iron walls are expected to be 5 m thick [8].

Downstream of the target there will be a muon shield.
.The muon shield will be $\sim$ 48 m long [8] and consists of magnetized iron [8]. The muon shield is designed to deflect muons with a momentum of up to 350 GeV [8] away, so they don't interfere with the experiment.

After the muon shield there is a neutrino target with a muon spectrometer in order to find more ν_τ events. The neutrino target itself consists of interleaved layers of emulsion film and lead plates assembled in bricks [8]. Each brick contains 57 thin emulsion films 56 lead plates of 1 mm thickness [8]. There will be 11 walls of 15×7 bricks [8], meaning that there will be a total thickness of lead in the target of 61.6 cm.
The neutrino target is encased in a "goliath" magnet with a magnetic field of up to 1.5 T [8].

The muon magnetic spectrometer consists of an array of straw tracker stations, a spectrometer magnet, that also serves as a calorimeter, and RPCs that are put in the gaps between the iron plates of the spectrometer magnet [8]. The setup of the neutrino target and the muon magnetic spectrometer can be seen in fig. 10.

Resistive plate chambers (RPC) are part of the muon magnetic spectrometer for the neutrino target [8] and are also used as veto taggers [15].
An RPC works in a similar fashion as many other types of micro strip gaseous chambers, containing an ionizable gas in a chamber with a high voltage applied so the electrons released in the gas will drift towards anode strips. Such chambers generally have a problem with generating sparks that break the detector and many designs are around to reduce this problem. In this case the problem is solved by letting the signal pas through a resistive plate whereafter the signal is then read out by copper strips. The gas gap itself is a couple of millimetres. In fig. 11 one can see a sketch of a typical RPC.

There are 22 layers of RPCs [8] with an efficiency for each RPC of 90 % [8],

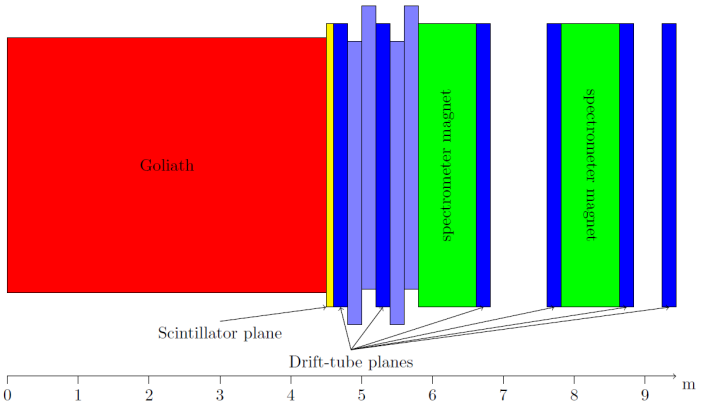

Figure 10: Neutrino target and muon magnetic spectrometer from [8]

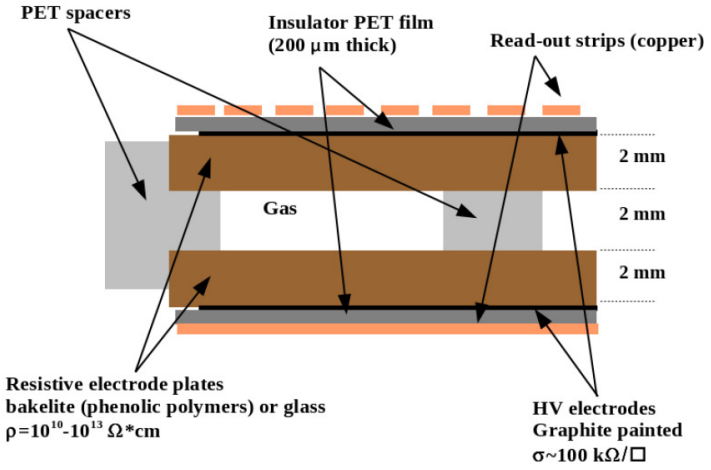

Figure 11: Resistive plate chamber [8]

giving a 10^{-22} probability of passing through all layers of RPCs undetected.

The following decay volume will be in a vacuum chamber; 62 m long [8], 5 m wide [8] and 10 m high [8] giving a 50 m long decay volume [8] where the last 12 m are used for the SHiP detector. In order to rule out background events, a number of veto taggers will be installed. The vacuum chamber is wrapped in a liquid scintillator detector [8], which is referred to as the surround background tagger or SBT, which has an estimated efficiency of 99% [8].

The upstream veto tagger is right in front of the entrance window to the vacuum chamber and is an array of plastic scintillator slabs with an expected efficiency of 99.9 % [8].

The straw veto tagger is 5 m down stream in the decay volume [8] and has an expected efficiency of 99.5 % [8].
The fiducial volume is the part of the decay volume between the straw veto tagger and the first straw tracker, which is the first part of the SHiP detector. The fiducial volume is illustrated in fig. 12.

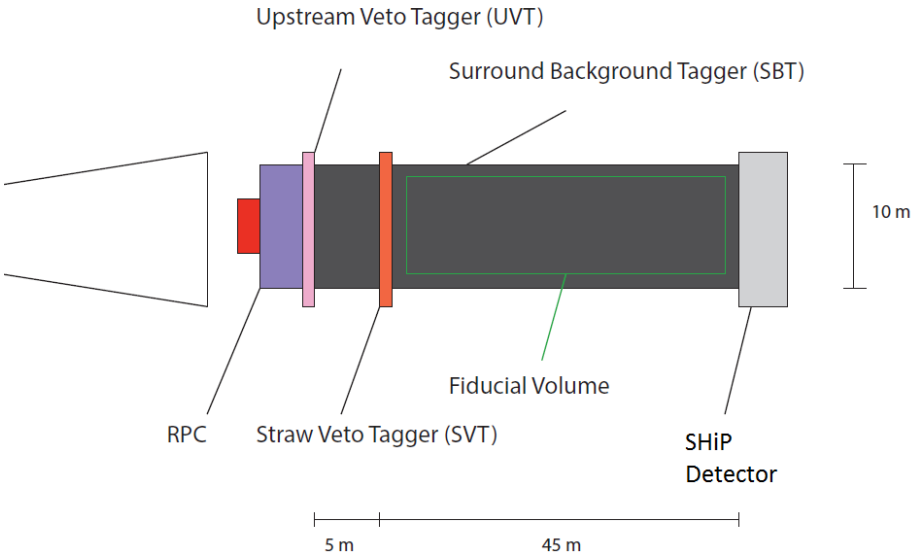

Figure 12: Sketch of the vacuum vessel of the SHiP experiment, with emphasis on the veto taggers.

The experiment is still in the design phase, but in this report, the setup of the experiment matches the one used in [8].

2.3 Other Searches with SHiP

The HNL search is far from the only search planned for the SHiP experiment. The abundance of ν_τ generated from the decays of heavy mesons will lead to detecting ~ 1000 of these in the neutrino detector, which is far more than the number of these particles observed until now. There will also be a large amount of $\bar{\nu}_\tau$, whereof it is expected to find half the amount of ν_τ. So far the $\bar{\nu}_\tau$ hasn't been observed, so the SHiP experiment could in principle be the first experiment to discover it.

The interesting particles for the SHiP experiment are particles beyond the Standard Model.
The SHiP experiment detects their Standard Model decay products, and based on the charactaristics of these decay products it can be deduced which particle they originate from.

2.4 Ship Software

The software for running simulations of HNL events in a configuration matching the SHiP experiment is called FairShip [17].

There are three steps in using FairShip: simulation, reconstruction and analysis.

The simulation has to do with all the particles and their interactions and is based on Monte Carlo (MC) [18] generators. The simulation of HNL events uses Pythia8 [19] to simulate the initial proton - target interactions. The decay of charmed mesons involving leptons is set to generate HNLs instead of neutrinos in Pythia8. [8]
The HNLs are followed through the experimental setup with Geant4 [20], wherein they are set to decay. The HNL decay products are then followed with Geant4 through the rest of the rest of the experimental setup. [8]

One can specify the decay modes to simulate in FairShip. The $HNL \to \pi\mu$ decay mode is set as default.

Neutrino interactions are simulated with Genie [21], where the interaction products are followed through the experiment with Geant4. [8]

The data from a simulation is stored in a geometry file and a file containg data about the particles in the simulation.

There are some important parts to note with the geometry: The coordinates for position are given in cartesian coordinates originating from the centre of the decay volume, where z runs along the beam axis, x is the transverse horisontal axis and y is the vertical axis.

The reconstruction deals with the detection of particles and the expected information stored in the detectors, and combines this information to reconstruct the particle tracks.

The analysis treats the data in the reconstruction to the specific needs by extracting data, performing the required operations and presenting the data in the required fashion. The analysis requires at least two input arguments in the same way as the reconstruction, where the output file from the reconstruction is used instead of the data from the simulation.

The important parts of the files to be analyzed are: The Monte Carlo tracks (MCtracks), The reconstructed tracks, and HNL candidates.
MCtracks are the tracks generated from the particles in the MC simulation, and one can access information on these tracks to get the "truth".

The reconstructed tracks contain information on each particle track based on its fitted parameters. Among these parameters are the momentum 3-vector and energy.

The HNL candidates are stored with the following information: Daughter particles, the momentum Lorentz vector, and the position Lorentz vector, where the time coordinate has been replaced by the distance of closest approach of the two daughter particles.

An event is defined to contain an HNL candidate if between 2 and 4 tracks form a vertex where at least one track has opposite charge from the others. The simplest case is where there are two tracks of opposite charge form a vertex and become an HNL candidate.
All possible combinations of two tracks of opposite charge that form a vertex in a given event are considered HNL candidates. This means that there can be multiple HNL candidates in a given event, so one has to make a loop over the HNL candidates in order to get information on all of them.

3 Analysis

This chapter contains the results of my work on estimating the HNL yield at a given mixing, U^2 and optimising the search for HNLs by improving the signal/background ratio.

3.1 HNL Signal

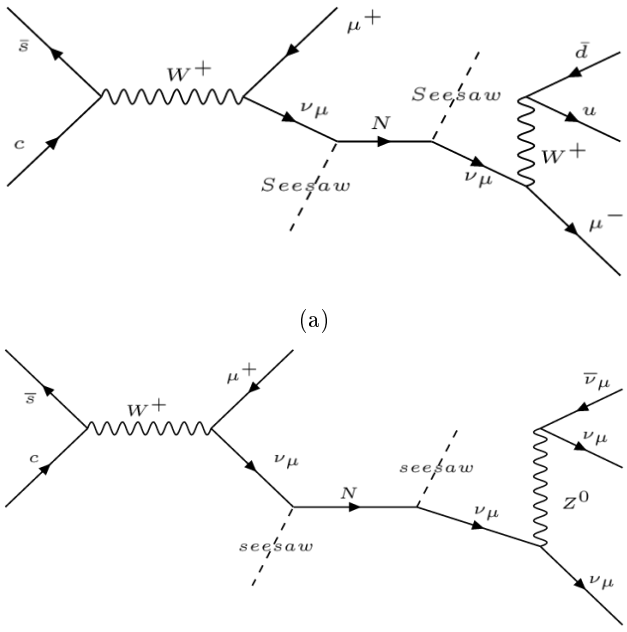

Figure 13: Feynmann diagram for the decay process of a Ds^+ meson creating an HNL and the subsequent decay process for the HNL into; $\pi^+ + \mu^-$ (a), and $\bar{\nu_\mu} + \nu_\mu + \nu_\mu$ (b)

Production of aa heavy neutral lepton (HNL) happens when a neutrino mixes into an HNL with the parameter U^2. This mixing can only happen if the mass difference between the initial meson and the decay products is larger than the mass of the HNL.

The only way an HNL can decay is by first mixing back to a neutrino. Since the HNL is much heavier than the neutrino, the neutrino will be in an excited state which immediately emits a W^+ - or a Z^0 boson. The mixing parameter U^2 is generally small, and therefore the lifetime is relatively large, which means that one needs a long decay volume in order to be able to detect any HNL decays.

When making a CP transformation, the decay processes for the antiparticles show up. These processes are also allowed.
When emitting a W^+, the neutrino becomes a lepton and W^+ will decay into a

positively charged meson or a neutrino - antilepton pair. The sum of the mass of the decay products has to be smaller than the HNL mass. An exaple is given on a process with production of an HNL from a D_s^+ decay and with its subsequent mixing and decay in the Feynmann diagram in fig. 13a.

The HNL decay into a pion and a muon shown in fig. 13a is an important HNL decay mode for many reasons. It is a dominant decay mode and all the decay products are detectable. This means that the $HNL \to \pi + \mu$ decay mode is of particular interest because one accurately reconstruct the mass of the HNL and destinguish it from background.

The emission of a Z^0 boson will result in the neutrino remaining a neutrino, while the Z^0 decays into a particle - antiparticle pair of either leptons or quarks. An example of such a process is given in fig. 13b, where the HNL decays into three neutrinos.

The mesons produced in the W^+ and Z^0 decays have a very short lifetime, except for π^+ [6], K_L^0 [6] and K^+ [6]. One expects to detect the decay products of the fast decaying mesons instead of the mesons themselves.

The expected production rate of HNLs for a proton-target collision in the SHiP experiment is found by using the following equation:

$$\chi(pp \to HNL) = 2 \cdot [\chi(pp \to c\bar{c}) \cdot BR(c \to HNL) + \chi(pp \to b\bar{b}) \cdot BR(b \to HNL)][8] \tag{11}$$

where $\chi(pp \to c\bar{c}) = 1.7 \cdot 10^{-3}$ [5] is the production rate for $c\bar{c}$. The term, $\chi(pp \to b\bar{b}) = 1.6 \cdot 10^{-7}$ [5] is the production rate for $b\bar{b}$, which only gives a minor contribution as long as the HNL is light enough to be created by most of the dominant charmed meson decays. $BR(c \to HNL)$ is interpreted as the branching ratio into a neutrino multiplied by $U^2\alpha$ where α is the neutrino flavour.

The HNL mixings to - and from the differnt neutrino flavours are chosen to be: $U_e^2 = 4.47 \cdot 10^{-10} : U_\mu^2 = 7.15 \cdot 10^{-9} : U_\tau^2 = 1.88 \cdot 10^{-9}$, which is similar to model 2 in [8], where the mixing between ν_μ and the HNL is maximized. The only difference is that U_τ^2 has been increased slightly. This choice of mixing angles will lead to a normal neutrino mass hierarchy.

The dominant modes for $BR(c \to HNL)$ are shown in the following equation:

$$\begin{aligned} BR(c \to HNL) = \sum_\alpha \Big[& BR(c \to D) \cdot BR(D \to K + \alpha + \nu_\alpha) \\ & + BR(c \to D_s) \cdot \big[BR(D_s \to \alpha + \nu_\alpha) \\ & + BR(D_s \to \tau\nu_\tau) \cdot [BR(\tau \to \alpha + \nu_\tau + \nu_\alpha) + BR(\tau \to \pi + \nu_\tau)] \big] \Big] \cdot U_\alpha^2 [8], \end{aligned} \tag{12}$$

where $\alpha = e, \mu, \tau$.

The branching ratios for the D mesons into final states with neutrinos are looked up in [6], and if the decay mode does not have enough invariant mass for the HNL and the remaining decay products, it is set to zero.

What remains is to find the branching ratios between the D mesons, which have been found using Pythia8 simulations in [5]. These values are given in table 3.

$BR(c \to D^+)$	0.3
$BR(c \to D^0)$	0.6
$BR(c \to D_s)$	0.08
$n(\tau)$	$3 \cdot 10^{15}$

Table 3: Branching ratios for the produced charm to the different charmed mesons and the number of produced τ from [5].

In the 1 GeV case the three flavours of $BR(c \to \nu_\alpha)$ are computed and shown in table 4. The relative errors are found to be: 5 % for ν_μ, 11 % for ν_e and 0.2% for ν_τ.

	1 GeV HNL	0.5 GeV HNL
$BR(c \to \nu_e)$	0.0989	0.1215
$BR(c \to \nu_\mu)$	0.0637	0.0992
$BR(c \to \nu_\tau)$	0.00479	0.00479

Table 4: Branching ratios for the produced charmed mesons to decay into neutrinos that can mix into HNLs.

To find the amount of HNLs decaying within a given volume, one would expect something like:

$$N_{HNL}^{decays} = N_{HNL} \cdot \left(1 - e^{-\Delta l / c\gamma\tau_{HNL}}\right) \tag{13}$$

With $\Delta l \approx 50$m and $\gamma\tau_{HNL} \approx 10^6$m, which is clearly a case of $\Delta l << \gamma\tau_{HNL}$, one can safely assume the 1st order approximation of the exponential function.

The expected amount of HNL events in the real experiment with the assumptions of 1 GeV mass and $U^2 = 9.5 \cdot 10^{-9}$ can then be calculated using the following equation:

$$n(HNL) = N(p.o.t)\chi(pp \to HNL)\frac{\Delta l}{c \cdot \tau_{HNL}}\gamma^{-1}[24], \tag{14}$$

where $n(HNL)$ is the number of HNL decays in the volume of the FairShip simulation, $N(p.o.t)$ is the number of protons on target, Δl is the length of the detector volume, c is the spped of light, τ_{HNL} is the HNL life time, $\chi(pp \to HNL)$ is the production rate of HNLs for a proton collision.

In order to use eq. 14 one has to determine τ_{HNL}.

The HNL lifetime is calculated using the total decay width of the HNL decays as follows:
$\tau_{HNL} = \hbar/\Gamma_{tot}$, where Γ_{tot} is the total decay width of the HNL.
The decay width of each possible decay mode is computed using equations from [24].
When these decay widths are computed, one has both the HNL lifetime and the branching ratios for the different decay products.

For an HNL with a mass of 1 GeV, $\Gamma_{tot} = 2.780 \cdot 10^{-21} GeV$ which leads to $\tau_{HNL} = 1.83 \cdot 10^{-4} s$.

With the production - and decay rate in place, one can now turn to the experiment to find out how many of the decays can actually be detected. For this purpose I will use simulations in FairShip to find the reconstruction efficiency of HNLs.

When using the simulation to find the probability for detection, it is also necessary to consider the distribution of simulated decays, which is found to be an even distribution over 70 m. The decay volume in SHip goes from the entrance window to the last tracking station of the vacuum vessel in SHiP. For simplicity, this length is taken to be 60 m. This means that the reconstruction efficiency from the simulation has to be scaled by 7/6 in order to be the experimental reconstruction efficiency.

$n(p.o.t)$	$2 \cdot 10^{20}$ [8]
$\chi(pp \to c\bar{c})$	$2.72 \cdot 10^{-3}$ [15]
Δl	60 m [8]

Table 5: Constants used to find the HNL yield

The Lorentz factor on the HNL is also found in the simulation by dividing the momentum of the HNL with its mass. This factor can be found in tables 6 and 9 for HNLs with a mass of 1 - and 0.5 GeV respectively.

In order to find the number of HNLs detected in the experiment, one has to multiply the result from eq. 14 with the reconstruction efficiency of the HNL decays and the branching ratio of the specific decay type searched for, so for the $HNL \to \pi\mu$ decay the expected yield would be:

$$N^{detected}_{HNL\to\pi+\mu} = n(HNL) \cdot BR(HNL \to \pi\mu) \cdot P_{rec}, \tag{15}$$

where P_{rec} is the probability for a decay to be reconstructed, given that the decay has happened within the decay volume.

FairShip is by default set to use a cascade production of charmed hadrons that can decay to HNLs instead of just using the direct production of these charmed hadrons. The HNLs will in this case have larger production angles,

and as a result a lower reconstruction efficiency.

The cascade process leads to an increase of charmed hadron production of $\sim 61\%$ [15]. The corrected value for $\chi(pp \to c\bar{c})$ is shown in tabele 5. Overall, including cascade production of charmed mesons will lead to an increase in reconstructed HNL events even though the reconstruction efficiency is reduced significantly.

One can find P_{rec} for different decay modes by running a simulation in FairShip and dividing the number of reconstructed events with the number of simulated decays scaled by a factor 7/6. The results on reconstruction efficiency from my simulations are found in table 7, along with my estimates for the branching ratios at 1 GeV.

$\chi(pp \to HNL)$	$2.785 \cdot 10^{-12}$
τ_{HNL}	$1.83 \cdot 10^{-4}$s
γ	23

Table 6: Values of HNL production rate, lifetime and Lorentz factor in the 1 GeV HNL mass case

One can find the HNL yield for the $HNL \to \pi\mu$ mode, using eq. 14 and 15 with the relevant values from tables 5, 6 and 7. This results in the estimate that 792 events in the $\pi\mu$ final state will be reconstructed as HNL candidates without any cuts applied.

To find the yield for another HNL decay mode, one simply chooses the values for that particular decay mode in table 7. As I have noticed in the simulations, the detection probability varies for the different decay modes (see table 7). This means that one has to run a simulation for each mode to have a more accurate estimate of the HNL yield in that particular decay mode. The resulting estimate of the HNL yield for the SHiP experiment is shown in table 8. Again it is emphasized that this yield is for the HNLs to be reconstructed before any cuts are applied.

In order to get an idea of how the full HNL yield will be at the benchmark scenario, a simulation with all decay channels open except for $HNL \to \nu\nu\nu$ has been made. The π^0 decay channel has also been included, so the reconstruction efficiency is a bit lower than it is supposed to be, since the tracking stations don't detect photons from the π^0 decay.
This however can be corrected by finding the π^0 branching ratio. With this correction, P_{rec} is found to be 19.8 %, while the branching ratio for the visible decay modes is 56.3 %. With this information, one can estimate the total number of expected HNL events as seen in table 8. The relative error on HNL production is at least 5 % from the branchings of charmed mesons, and if on assumes a similar error on the HNL decay rate and branching ratios, one has a relative error of 9 % for the expected HNL yield.

If one keeps U^2 fixed, but switches to a lighter HNL at 0.5 GeV instead,

Decay mode	Branching ratio	P_{rec}
$HNL \to \pi^+ + \mu^-$	16.03 %	0.187
$HNL \to e^- + \nu + \mu^+$	9.72 %	0.175
$HNL \to \mu^- + \nu + \mu^+$	4.84 %	0.21
$HNL \to visible$	56.3 %	0.198
$HNL \to \pi^0 + \nu$	11.7 %	0
$HNL \to \nu + \nu + \bar{\nu}$	12.2 %	0

Table 7: Branching ratios and reconstruction efficiencies for decay modes with an HNL mass of 1 GeV

HNL mass	HNL decay mode	HNL yield
1 GeV	$N^{detected}_{HNL\to\pi+\mu}$	792
	$N^{detected}_{HNL\to\mu+\mu}$	270
	$N^{detected}_{HNL\to e+\mu}$	450
	$N^{detected}_{HNL\to visible}$	2962
0.5 GeV	$N^{detected}_{HNL\to visible}$	189

Table 8: Expected HNL yield of the SHiP experiment, given a normal neutrino mass hirarchy with $U^2 = 9.5$

$\chi(pp \to HNL)$	$4.203 \cdot 10^{-12}$
τ_{HNL}	$c \cdot 4.92 \cdot 10^{-3}$
γ	16.3
$BR(HNL \to \pi^0 + \nu)$	34.9 %
$BR(HNL \to visible)$	54.9 %
$P^{visible}_{rec}$	0.143

Table 9: Parameters from the HNL with 0.5 GeV mass that are needed to estimate the number of HNLs detected in the ship experiment.

some of the parameters change. The HNL lifetime is increased, the momentum is reduced, the subsequent decay products have different branching ratios and the reconstruction efficiency can hence not be assumed to be the same. The production rate of HNLs increase since more charmed meson decays are allowed as seen in table 4. These new parameters are shown in table 9.
One then uses the parameters from tables 9 and 5 in eq. 14 and 15 to find the expected HNL yield, which can be found in table 8.

3.2 Neutrino Background

From $2 \cdot 10^{20}$ Protons on target, there should be about $4 \cdot 10^{17}$ neutrinos and $3 \cdot 10^{17}$ anti neutrinos within 100 mrad of the beam axis according to [8]. These are mainly muon neutrionos, so when neutrinos are mentioned in this section, it is implied that they are muon neutrinos.
100 mrad is a reasonable limit for estimating the neutrino background, since the distance from the target to the neutrino target is 54 m, the neutrino flux will then be ~ 5.4 m from the beam axis. It means in priciple that there might still be some interactions with the corners of the muon shield, but the angle only has to be increased by $\sim 10\%$ to be clear of these, and beyond this point, any neutrino flux is outside the reach of any detectors in the experiment.
Since neutrinos only interact in weak interactions, which has a very small cross section, only 10^7 out of $4 \cdot 10^{17}$ neutrinos interact with material in - and around the decay volume.
It is expected that inelastic scattering from these weak interactions will result in the reconstruction of $\sim 3 \cdot 10^4$ HNL candidates [15] that leave two tracks originating from particles of opposite charge. The anti-neutrinos are expected to contribute with one third of that number due to a smaller cross section.
The neutrino scattering processes result in either a muon and hadrons or just hadrons depending on whether the interaction is by charged current or by neutral current.

In simulations, one can skip all the events that don't interact. This means that it is managable to get enough statistics to match the $2 \cdot 10^{20}$ protons on target. Since this background involves many reconstructed HNL candidates, one can compare these events with HNL signal.

The neutrino background data used in this analysis has a distribution in polar angle seen in fig 14, which peaks well within 100 mrad, but with a significant tail outside 100 mrad. This means that one can expect a slightly lower reconstruction efficiency than what one can expect from the same number of interactions in the experiment.

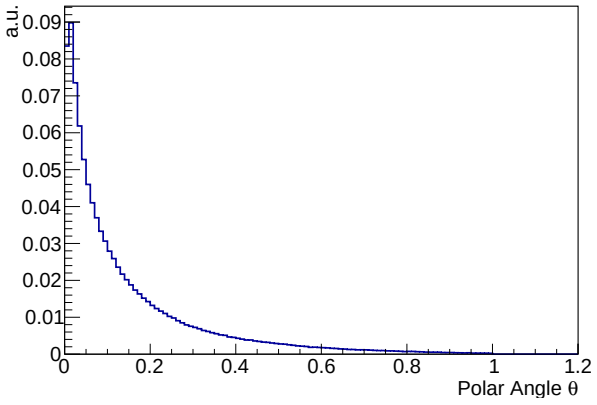

Figure 14: Distribution of neutrino polar angle from MC simulation

The reconstruction efficiency for the neutrino background is 0.27 %, while it for antineutrinos is 0.17 % in the neutrino files used.

3.3 Muon Background

The muon background can be divided into three categories: Inelastic scattering, combinatorial, and cosmic background. The inelastic scattering process for muons can generate hadrons that decay into particles that can be detected as a fake HNL event.
These scattering processes both happen in the concrete walls surrounding the SHiP experiment and near the entrance to the vacuum vessel. The amount of interractions near the entrance to the vacuum vessel should match the amount of neutrino interactions. The interactions with the concrete wall require a lot of statistics because it involves the muons deflected by the muon shield.

The combinatorial background hasn't got any statistics, but has been calculated to be less than 0.1 [15]. The frequency of muon tracks in the detector area can be decreased by imposing a cut on momentum. Thereby also decreasing the probability of creating a fake event.

The cosmic background has good statistics and is a small contributor to the background, mainly because the impact parameter is larger that 10 m [15].

In the following analysis, the muon background is assumed to be negligible compared to the neutrino background.

3.4 Selection Cuts

In order to ensure valid data and increase the signal/background ratio, it is necessary to apply some cuts on the selection of HNL candidates. Some of the cuts are on parameters where there is some difference in distribution of signal and background.

In fig. 15, the distributions of the $HNL \to \pi + \mu$ signal match the plots from [8], but for the neutrino background there is a peak at 30 degrees of freedom in fig. 15c, which is much smaller in [8]. The vertex z position is also distributed differently than in [8], with more events upstream for the neutrino background in fig. 15e. Apart from these two details, there is consistencey with [8]. In addition to the plots in fig. 5.17 in [8], a plot over the momentum ditribution of the decay products has been added (see fig. 15d). Furthermore, the mass distribution of the neutrino background has been added to the plot in fig. 15f.

In fig. 16, the same set of variables is shown for an HNL signal with a mixture of final states matching what one expects in the real experiment if the HNL has a mass of 1 GeV. The fraction of the $HNL \to \pi + \mu$ decays is 27 %. The distributions of the anti neutrinos in fig. 16 match the neutrino distributions in fig. 15.

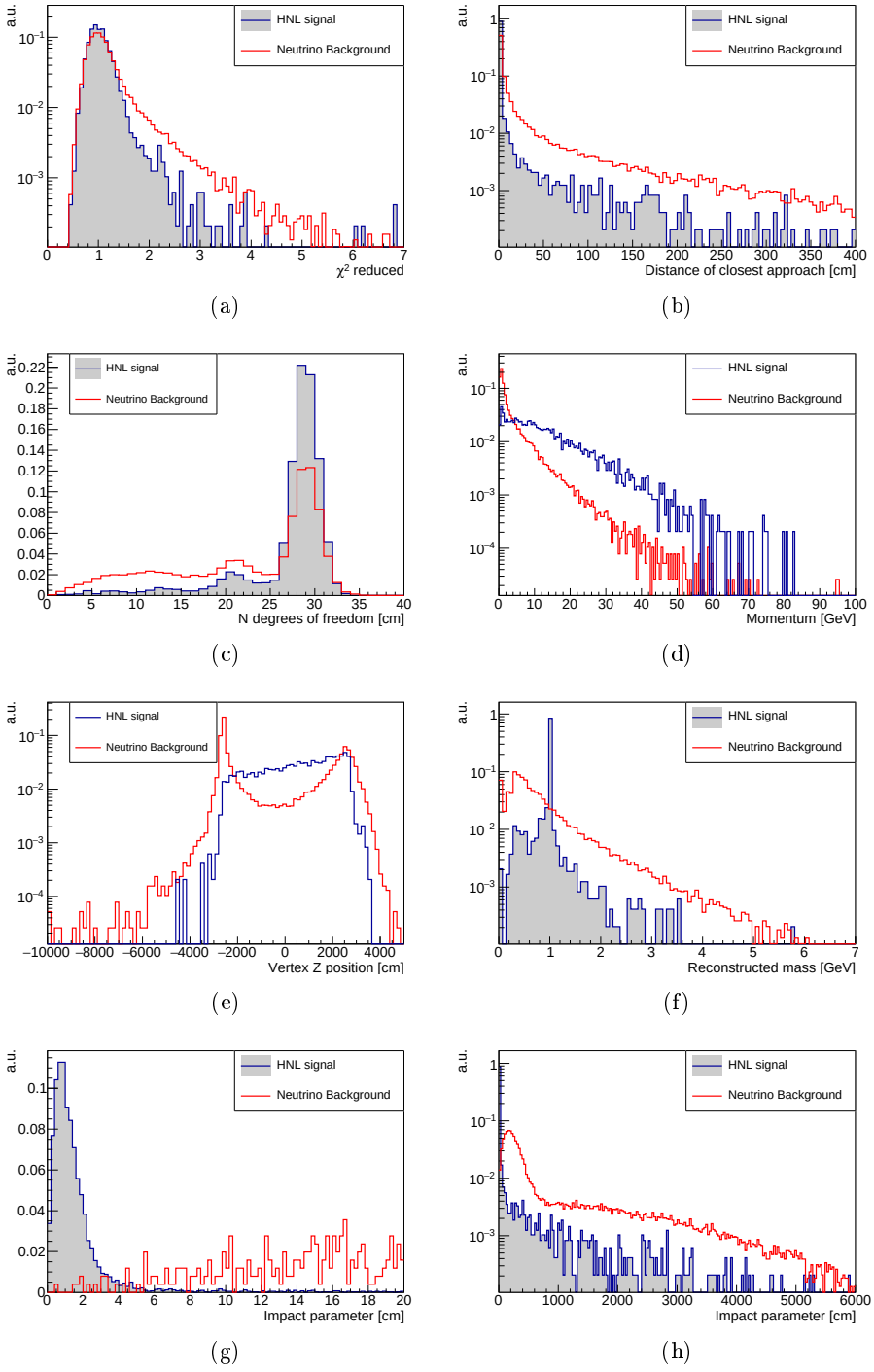

Figure 15: Distribution of selected variables for the $\pi + \mu$ final state of the HNL and the neutrino background at the reconstruction

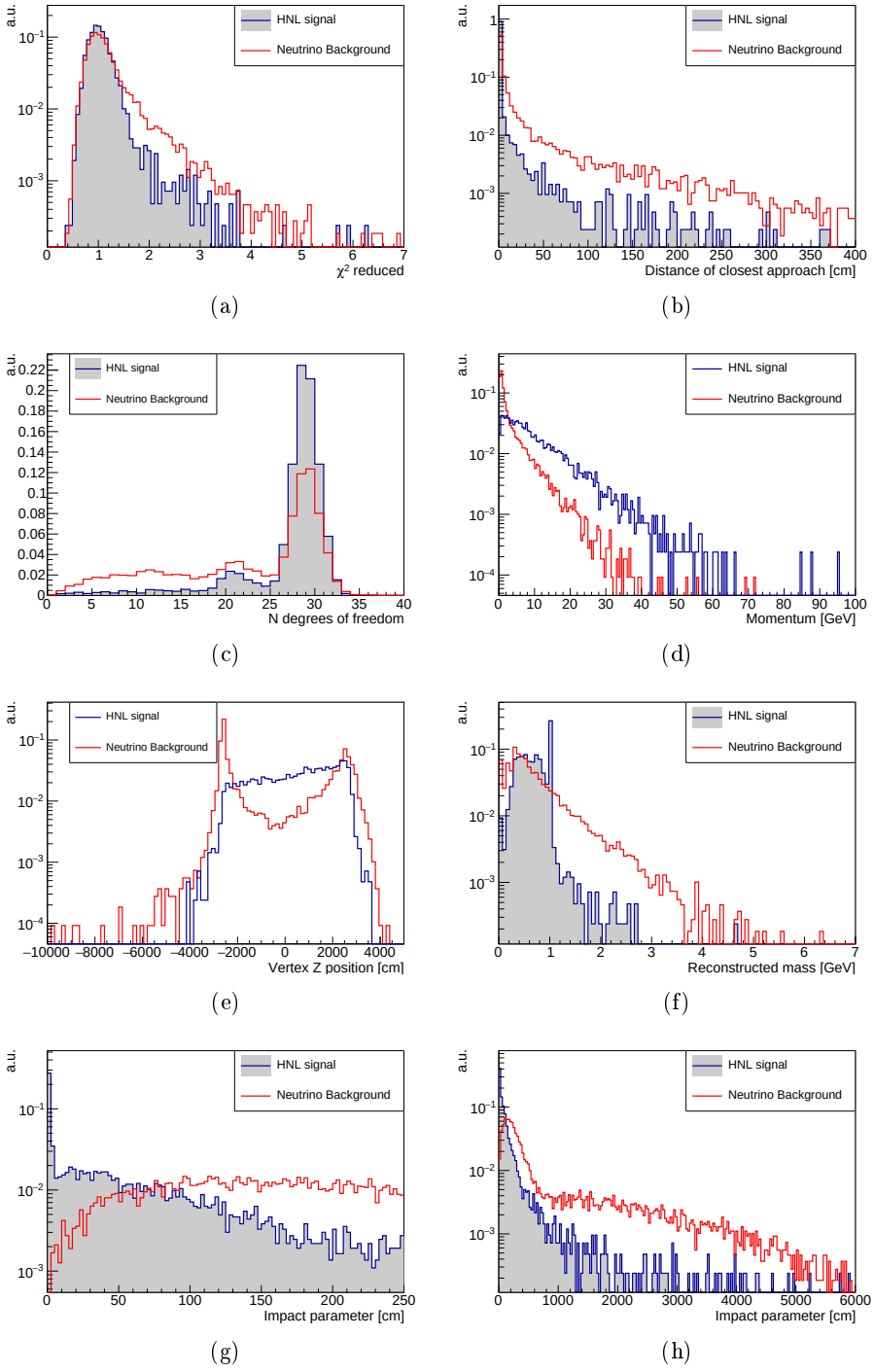

Figure 16: Distribution of selected variables for mixed final state of the HNL and the anti-neutrino background at the reconstruction

3.5 Cuts proposed by the SHiP Collaboration

The following cuts are the same as the ones given in [15]: Starting with the total number of reconstructed HNL candidates.
The reconstruction criteria for an event is explained in section 2.4.

Removing HNL candidates from events with multiple HNL candidates.
This is done to reduce background, since scattering processes from background are likely to make hadron showers with more than two particles.

Requiring the vertex to be within the fiducial volume(behind the straw veto tagger within the vacuum tank).
This will rule out background events that managed to get through the veto detectors undetected. The fiducial volume is set to be between the straw veto tagger and the first straw tracker station with 20 cm to the centre of both the straw veto station and the first tracking station as illustrated in fig. 12. It is also required that the vertex lies within the walls of the vacuum vessel with a 1 cm error margin.

Requiring both tracks to be within the fiducial volume.
The tracks are also required to be inside the walls of the vacuum chamber in order to rule out cosmics or other events going through the SBT without triggering it.

Degrees of freedom greater than 25.
This rules out tracks that don't hit all tracking stations, which the background is more likely to do than the signal. This also ensures the track is accurately reconstructed so that one can find things like vertex location ,impact parameter and the invariant mass of the mother particle.

DOCA less than 1 cm after recalculating the vertex.
The Doca can be calculated using the following equation:

$$Doca = \vec{PQ} \cdot \vec{u} \times \vec{v}/|\vec{u} \times \vec{v}|[17] \tag{16}$$

Where P is a point in the first track and Q is a point in the other track, $\vec{u}$ is the momentum vector of the first track while $\vec{v}$ is the momentum vector for the other track. The equation is the projection of the vector going from a point in one line to a point in the other unto the unit normal vector of the plane spanned by the direction vectors of the two tracks.

In the analysis, however the Doca is defined as the distance between the two points at the vertex, which is then optimised in an iterative process. The advantage of this method is to find both the DOCA and the vertex position, which is used in the fiducial cuts. The initial guess for the vertex follows the equation for P:

$$P = P_0 + (\vec{PQ} \cdot \vec{v} - (\vec{PQ} \cdot \vec{u})(\vec{u} \cdot \vec{v}))/(1 - (\vec{u} \cdot \vec{v})^2)P[17] \tag{17}$$

Where P_0 is the trackposition at the detectors. For Q the procedure is identical. In new reconstructions of simulations, the DOCA is stored where the time shoult

have been in the position 4 vector.

Reduced chi squared less than 5.
This ensures that the reconstructed track is reasonably fitted and by itself this cut generally has an efficiency of 100%, meaning that all signal - and background events that pass the previous cut are within the accepted limit.

Both daughter tracks have momentum higher than 1 GeV/c.
This requirement is intended to reduce the frequency muon background that will be accepted as HNL candidates, since most of the muons will have low momentum after passing through the muon shield. It will also rule out some of the neutrino background.

Impact Parameter less than 10 cm for $\pi\mu$ decay and 250 cm for other decays.
The impact parameter with regards to the target is calculated as follows:

$$Ip = \sqrt{\sum_i ((x_i - x_{i0}) - v_i \cdot t)^2} \tag{18}$$

where x_i is the coordinate of the point on the ith axis, while x_{i0} is the coordinate on the ith axis of the target. In the simulations it should be noted that the time is not accessible, so one has to work around this issue.

No hits in any veto detector.
Most neutrino events trigger at least one veto detector, unless they iteract with material inside the decay volume where there are no veto taggers. Since HNLs don't interact with any material and can decay anywhere, including in vacuum beyond the veto taggers. Muons will in general trigger veto detectors unless they are generated inside the fiducial volume or slip through due to inefficiency of the veto detector.

3.6 Application of Cuts to HNL Signal and Neutrino Background

I have applied the cuts explained above to different sorts of HNL signal along with neutrino background, where the results are put in the tables below. I made the HNL signal in simulations, while the neutrino background has been simulated in advance due to the high number of events and the low reconstruction efficiency.

For the tables containing HNL signal there is a column labeled "Experiment" which is an estimate of the expected HNL signal in that particular HNL decay mode found in section 3.1.

	Selection	Efficiency	Experiment
Simulated events	30000		
Reconstructed events	4836	16.1%	792
1HNL	4542	93.9%	744
Vertex in fiducial volume	3882	85.5%	636
Tracks in fiducial volume	3499	90.1%	573
N.d.f. > 25	3325	95.0%	545
DOCA < 1 cm	3113	93.6%	510
$\chi^2/N.d.f. < 5$	3113	100.0%	510
Daughters P>1 GeV	3105	99.7%	509
IP < 10 cm	3082	99.3%	505
Not Vetoed	2964	96.2%	485

Table 10: Cut efficiencies for HNL decay into $\pi^+ + \mu^-$

One can compare the efficiencies in table 10 with table 2.1 in [15] and find that they are in agreement within 5%.

	Selection	Efficiency	Experiment
Simulated events	10000		
Reconstructed events	1821	18.2%	269
1HNL	1821	100.0%	269
Vertex in fiducial volume	1477	81.1%	218
Tracks in fiducial volume	1268	85.8%	187
N.d.f.>25	1214	95.7%	179
DOCA<1 cm	1110	91.4%	164
$\chi^2/N.d.f. < 5$	1110	100.0%	164
Daughters P>1 GeV	1107	99.7%	164
IP<250 cm	1018	92.0%	150
Not Vetoed	1017	99.9%	150

Table 11: Cut efficiencies for HNL decay into $\mu^+ + \mu^-$

	Selection	Efficiency	Experiment
Simulated events	10000		
Reconstructed events	1495	15.0%	450
1HNL	1485	99.3%	447
Vertex in fiducial volume	1310	88.2%	394
Tracks in fiducial volume	1208	92.2%	364
N.d.f.>25	1146	94.9%	345
DOCA<1 cm	1033	90.1%	311
$\chi^2/N.d.f. < 5$	1033	100.0%	311
Daughters P>1 GeV	1025	99.2%	309
IP<250 cm	940	91.7%	283
Not Vetoed	935	99.5%	281

Table 12: Cut efficiencies for HNL decay into $e + \mu$

	Selection	Efficiency	Experiment
Simulated events	30000		
Reconstructed events	4188	14.0%	2962
1HNL	3945	94.2%	2790
Vertex in fiducial volume	3333	84.5%	2357
Tracks in fiducial volume	3072	92.2%	2173
N.d.f.>25	2874	93.6%	2033
DOCA<1 cm	2614	91.0%	1849
$\chi^2/N.d.f. < 5$	2613	100.0%	1848
Daughters P>1 GeV	2598	99.4%	1837
Ip<10 cm (IP<250 cm)	939 (2466)	36.1% (94.9%)	664 (1744)
Not Vetoed	907 (2328)	96.6% (94.4%)	641 (1646)

Table 13: Cut efficiencies for HNLs with 1 GeV mass decaying into visible final states

In table 15 the column labeled "Experiment" starts out with the number of reconstructed neutrino final states in [15], which is about 14% more than what one expects from a 10^7 neutrino events of the analyzed data.

When arriving at the Ip cut in table 15, one has a number of remaining HNL comparable to the values from [15], however there are some of the cuts with efficiencies that differ significantly from what is seen in [15], especially 1 HNL, N.d.f.>25, P>1 GeV and Ip $<$ 250 cm. The anti-neutrinos in table 16 appear to be slightly more resilient to the cuts applied. The response to each cut is similar for the anti-neutrinos and since they are still less than the neutrinos, this effect would hardly be a problem.

Tightening the cut on impact parameter to only select events with an impact parameter less than 10 cm would rule out the $HNL \to \mu + \mu$ decays and the $HNL \to e + \mu$ decays and thus reducing the HNL signal, but the neutrino background would be suppressed to 0 according to the data used here, and 0.2 according to [15] before the veto cut.

	Selection	Efficiency	Experiment
Simulated events	30000		
Reconstructed events	2800	9.3%	189
1HNL	2689	96.0%	182
Vertex in fiducial volume	2254	83.8%	152
Tracks in fiducial volume	2040	90.5%	138
N.d.f. > 25	1936	94.9%	131
DOCA < 1 cm	1737	89.7%	117
$\chi^2/N.d.f. < 5$	1736	99.9%	117
P>1 GeV	1726	99.4%	117
IP < 10 cm (< 250 cm)	1439 (1720)	83.4% (99.7%)	97 (116)
Not Vetoed	1388 (1668)	96.5% (97.0%)	94 (113)

Table 14: Cut efficiencies for HNLs with 0.5 GeV mass decaying into visible final states

	Selection	Efficiency	Experiment
Simulated events	$1.4 \cdot 10^7$		
Reconstructed events	38386	0.27%	31162[15]
1HNL	20688	53.9%	16795
Vertex in fiducial volume	4590	22.2%	3726
Tracks in fiducial volume	3558	77.5%	2888
N.d.f.>25	1346	37.8%	1093
DOCA<1 cm	192	14.3%	156
$\chi^2/N.d.f. < 5$	192	100.0%	156
Daughters P>1 GeV	153	79.7%	124
IP < 10 cm (< 250 cm)	0 (80)	0% (52.3%)	0 (65)
Not Vetoed	0 (< 1)	$< 1.3\%$	0 (< 0.79)

Table 15: Neutrino background with cuts applied

	Selection	Efficiency
Simulated events	$6.4 \cdot 10^6$	
Reconstructed events	11022	0.17%
1HNL	6422	58.3%
Vertex in fiducial volume	1375	21.4%
Tracks in fiducial volume	1078	78.4%
N.d.f.>25	399	37.0%
DOCA<25 cm	76	19.0%
$\chi^2/N.d.f. < 5$	76	100.0%
Daughters P>1 GeV	64	84.2%
IP < 10 cm (< 250 cm)	0 (34)	0% (53.1%)
Not Vetoed	0 (< 0.4)	<1.2%

Table 16: Anti neutrino background with cuts applied

One can find the upper bound on the neutrino background by identifying the cut that performs the worst in connection with the veto. That cut turns out to be the cut on Doca, where the efficiency for passing the veto cut is 1.2 %.
This means that one can set the upper bound on the neutrino background by assuming one event passing all cuts up to the veto, meaning that one can expect about 0.012 events passing the veto cut when the cut on impact parameter is set to 10 cm.

3.7 Methods for Multivariate Analysis

So far the cuts used are simple rectangular cuts, and it is possible that the cuts can perform better when set at other values. The correlations between the variables used for cuts could lead to an alternate method to cuts being more efficient. I have chosen three methods to compare: Rectangular cuts, likelihood (LLH), and boosted decision trees (BDT).
These methods are compared, when using a sample of neutrino background together with either of the following decay modes: $HNL \to \pi\mu$, $HNL \to \mu\mu$ or a mixed HNL signal, all with an HNL mass of 1 GeV.
The variables used in the optimisations are: Distance of closest approach (Doca), reduced χ^2 (Chi2), momentum (P), and impact parameter (Ip).

To optimize I use TMVA [22], which is built in in ROOT [23] to deal with multivariate analysis. It takes in trees or ASCII files as input where the same variables exist for both signal and background. The input is divided in to a test - and a training sample, where the training sample is used to find the optimal cuts to distinguish signal from background using a given method, while the test sample is used to apply the cuts found from the training sample. The optimisation is done using $S/\sqrt{S+B}$ which depends on the initial signal/background ratio and scales with the square root of the amount of signal.

The parameter that one wants to optimize in SHiP is U^2, which one wants to minimize in the limit for $S = B + 3 \cdot \sigma_B + 1.6 \cdot \sigma_S$.
$U^2 \propto \sqrt{S^{-1}}$, which should then be multiplied with $\sqrt{\frac{B+3\cdot\sigma_B+1.6\cdot\sigma_S}{S}}$ to get the minimal value of U^2. Minizing U^2 is then the same as maximizing the ratio: $\frac{S}{\sqrt{B+3\cdot\sigma_B+1.6\cdot\sigma_S}}$. This is not quite the parameter $S/\sqrt{S+B}$ used in TMVA, unless one is in the limit: $S \ll B$.
When reaching low values of background in the optimization σ_S starts to act more or less as a constant, so one can set it to $\sigma_S = 2$. One can find an approximate value for $B+3\sigma_B$ in the low limit to be $B+3\sigma_B \approx 2\cdot B+3$, which means that one can optimize the value $\frac{S}{\sqrt{2\cdot B+5}}$. One can then use the appropriate value for S to make the optimsation relevant to U^2, which is set to be 9.

3.7.1 Cuts

TMVA applies cuts on the variables that leave behind a certain amount of the signal while optimizing the background rejection. This process is repeated for each amount of signal to leave behind until the predefined number of cut attempts have been used. In this case the number of attempts is set to $4 \cdot 10^6$, which takes a couple of minutes to compute.
The distribution of some of the variables are seen in fig. 17 as they are displayed in TMVA. The logarithm has been taken of the Doca in order to ease fitting of this variable.

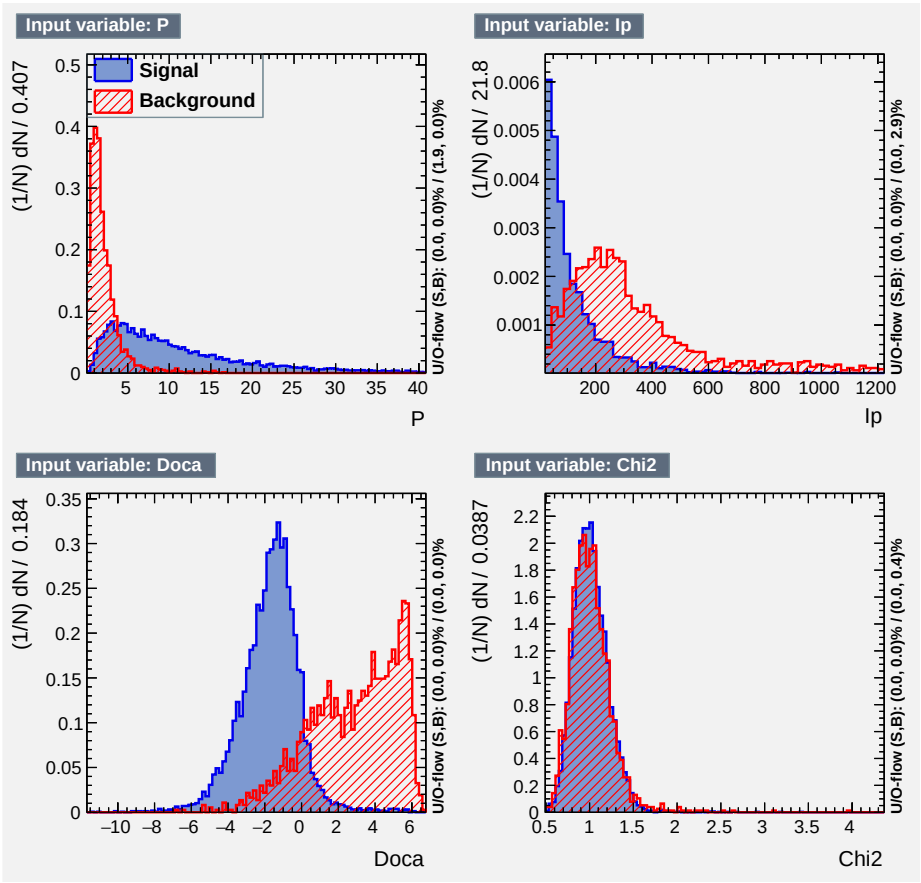

Figure 17: Distributions of variables for mixed HNL signal at 1GeV from TMVA

3.7.2 Likelihood

With the likelihood method, histograms of the training samples are fitted with a probability density function (PDF), which is used to determine the likelihood of the test sample. Making good fits of the histograms for each variable is important for this method to work optimally, so it will be important to adjust binning of the histograms to be fitted.

The likelihood is calculated as follows:

$$likelihood = -\log(\frac{ps + pb}{ps} - 1)/15[22],$$

where ps is she probability for the event being a signal, calculated by multiplying the probability density for each variable, pb is the probability of the event being background. In fig. 18 the likelihood distribution for the selected set of variables is shown. The huge spaces between the peaks are due to the fact that the tails of the PDFs are rather short, so when the space between datapoints in the tail grows too large, the PDF takes a zero value which corresponds to a jump of around 2 in the likelihhod scale - if the PDF for the other dataset is still nonzero.

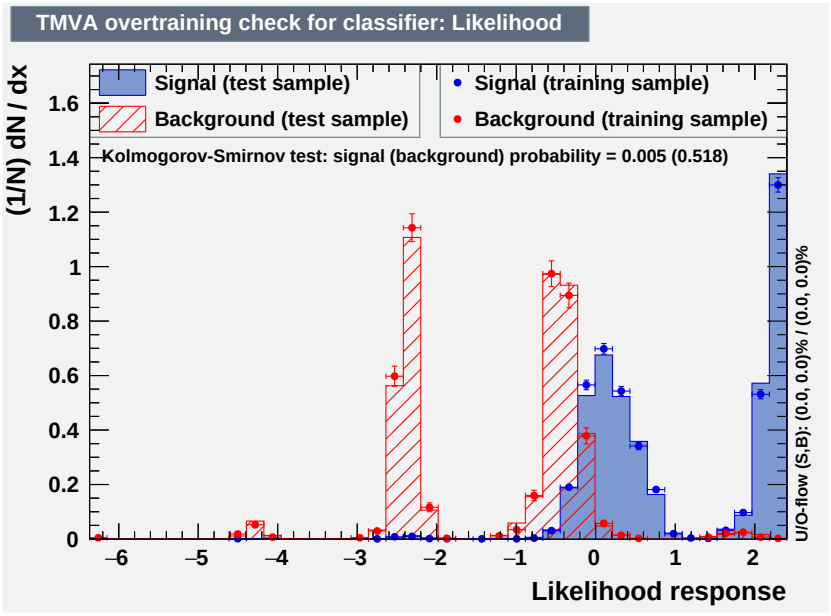

Figure 18: Likelihood distribution for signal and background - the filled histogram is the test sample while the errorbar plot is for the training sample

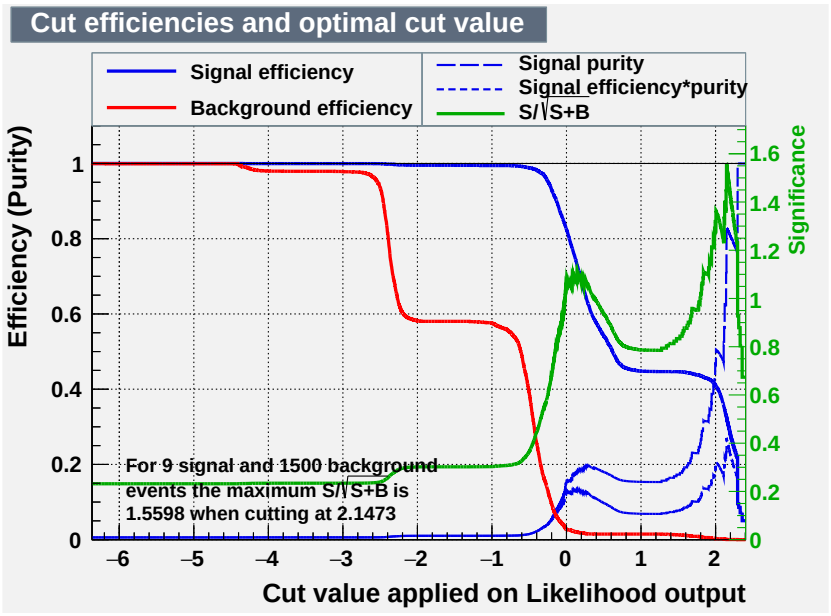

Figure 19: Optimisation of likelihood cut

When using the likelihood method, it is important to check the correlations between the variables. Ideally the variables are supposed to be uncorrelated for this method to be optimal. In fig. 20 we find the linear correlations. In this

case where there is a strong linear correlation between P and Ip in the signal. It has been attempted to use an option for the likelihood method to use variable transformations in order to decorrelate them, but it does not seem to have any effect. This is because the linear correlations also have nonlinear elements that can not be removed by trivial transformations.
The optimisation for mixed HNL signal is shown in fig. 19.

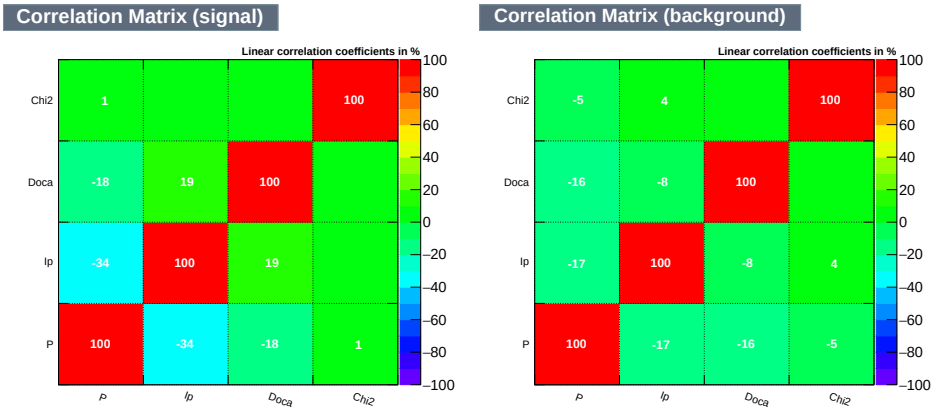

(a) Linear correlations in signal in % (b) Linear correlations in background in %

Figure 20

3.7.3 Boosted Decision Tree

The boosted decision tree or BDT is an other tool to distinguish signal from background. In order to understand this method, one has to first look at a simpler case, namely the decision tre. The decision tree selects a cut on a variable, where a yes/no decision is made. This process is the repeated both for the yes and no response with new cuts on new variables. When all steps in the decision tree are taken, the datapoint is either classified as signal or background.

A boosted decision tree makes a lot of small decision trees following a selected algorithm. The algorithm used in this case is called AdaBoost [22]. Every decision tree is weighted according to its ability to split signal from background, following the relation $\alpha = \beta \cdot \log(\frac{1-err}{err})$[22], where α is the weight, β is the learning rate and err is the error which goes from 0, in case of perfect seperation of signal and background in a single decision tree, to 0.5 where the new decision tree does not separate signal from background at all.

The output is then the sum of the weights identifying the event as signal minus the sum over weights identifying the event as background. The result is then divided by the number of decision trees.
The distribution for signal and background after using decision trees can be seen in fig. 21. The most important thing to check is if there is consistensy between the distribution of the training - and test sample. If these distributions are inconsistent, some overtraining is involved, which reduces performance of

the optimisation significantly.
The optimisation to $S/\sqrt{S+B}$ is shown in fig. 22.

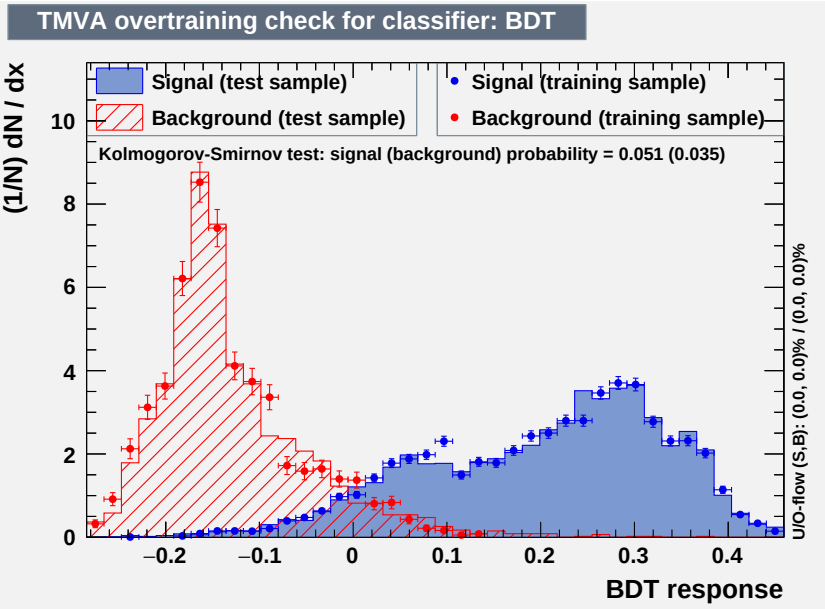

Figure 21: Boosted decision tree distribution for signal and background - the filled histogram is the test sample while the errorbar plot is for the training sample with mixed HNL signal

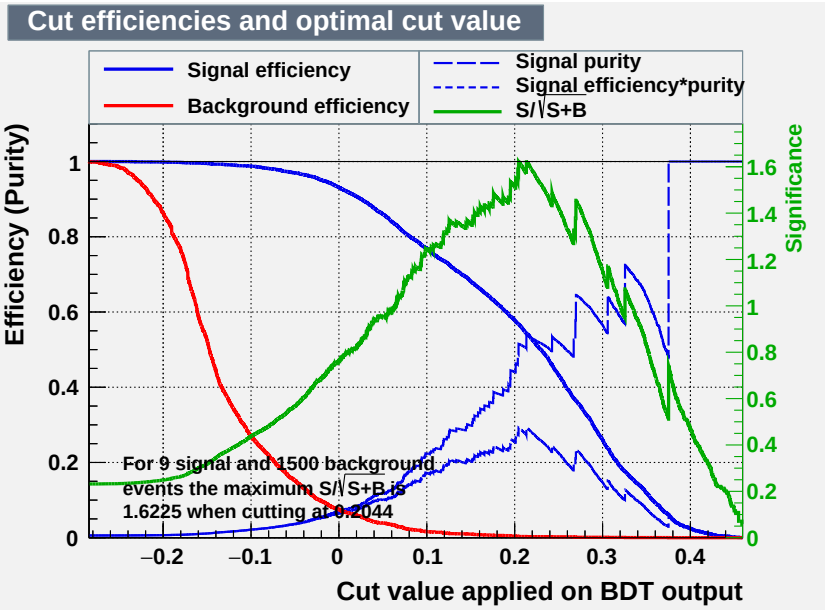

Figure 22: Boosted decision tree cut optimisation for mixed HNL signal

Method	Optimal Cut	$S/\sqrt{S+B}$	NSig	NBg	EffSig	EffBg
Likelihood	0.2257	2.505	8.494	3	0.9438	0.002
Cuts	0.945	2.922	8.536	0	0.948	0
BDT	0.1492	2.754	8.64	1.2	0.960	0.0008

Table 17: Using $HNL \to \pi + \mu$ HNL signal with 1 GeV mass

Method	Optimal Cut	$S/\sqrt{S+B}$	NSig	NBg	EffSig	EffBg
Likelihood	2.0462	1.37	2.7	1.2	0.3017	0.0008
Cuts	0.5050	1.45	4.6	5.4	0.5085	0.0036
BDT	0.1424	1.32	3.9	4.8	0.4321	0.0032

Table 18: Using $HNL \to \mu + \mu$ signal with 1 GeV mass

3.7.4 Evaluation of TMVA methods

There seems to be no remarkable difference in cut efficiency between using cuts and using either likelihood or BDT, as seen in fig. 23. In fact using cuts is slightly better than the other methods in the region where the optimisation takes place (as seen in tables 17, 18 and 19).

One can see in table 18 that about 50 % of the $HNL \to \mu + \mu$ signal will remain after optimizing the cuts. There will still be 5 to 6 background events remaining after these cuts, meaning that after applying the veto cut as well, one would have around 0.072 background events. This is within the goal of 0.1 background events.

When using data from all the visible HNL decay modes combined, the cuts give a slightly better signal/background ratio compared to the $\mu+\mu$ decay mode as seen in table 19. The signal still has around 56 % of the events left, and the background is douwn to 3 events before the veto, meaning around 0.04 background events after the veto.

The cuts from the optimisation on the different samples of HNL data are shown in table 20. For the $HNL \to \pi + \mu$ signal, the cut on momentum is very close to where it is suggested in [15], while the cut on impact parameter goes down to 3.6 cm. The cut on Doca is practically ignored in this case. The signal acceptance in this case will at 94 % be 5 % higher than when using the cuts suggested in [15], while the background is removed just as efficiently. The cut on impact parameter will kill any signal originating from other deacay modes than $HNL \to \pi + \mu$ though.

Method	Optimal Cut	$S/\sqrt{S+B}$	NSig	NBg	EffSig	EffBg
Likelihood	2.117	1.66	2.77	0	0.3076	0.0000
Cuts	0.5550	1.77	5.0	3	0.5576	0.002
BDT	0.1277	1.42	5.4	9	0.5969	0.006

Table 19: Using mixed HNL signal with 1 GeV mass

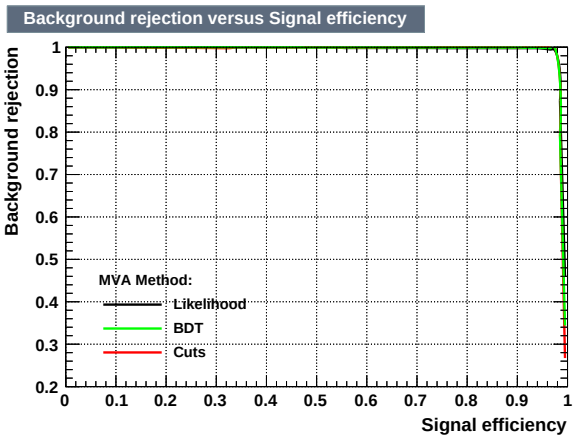

(a) Comparison of TMVA methods on $\pi\mu$ signal

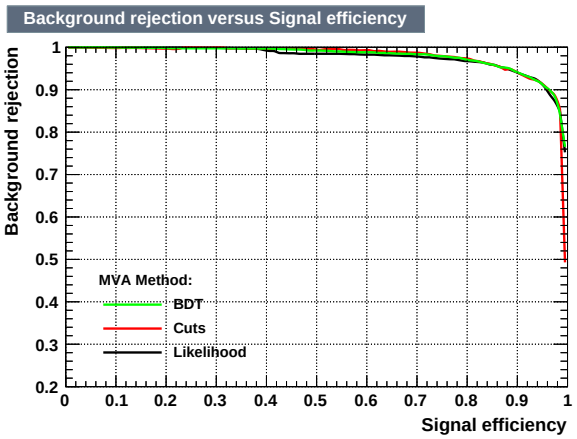

(b) Comparison of TMVA methods on $\mu\mu$ signal

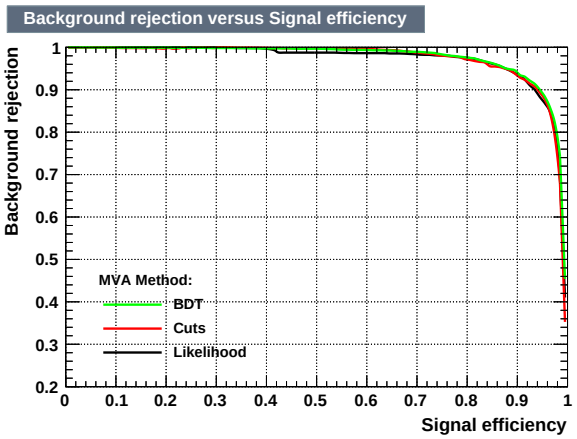

(c) Comparison of TMVA methods on mixed HNL signal

Figure 23

Signal	P [GeV]	Ip [cm]	Doca [cm]	$\chi^2/N.d.f$
$HNL \to \pi + \mu$	> 0.93	< 3.6	< 454	< 5
$HNL \to \mu + \mu$	> 4.9	< 88	< 2.86	< 5
Mixed HNL decays	> 5.21	< 78	< 2.6	< 2

Table 20: Cuts from TMVA optimisation on differt types of HNL signal with 1 GeV mass

The cuts from optimisation on the mixed HNL - and the $HNL \to \mu + \mu$ signal are very close to each other, where the cut on momentum is about 5 GeV, which is relatively high. This might cause problems for low mass HNL signal, since momentum increases with the HNL mass.

So far the cuts have only been optimized for an HNL mass of 1 GeV while it in principle can range from 0.18 to 5 GeV and still be relevant for this experiment.

3.8 Particle Identification

Destinguishing particle final states opens up for possibilities to increase the signal/background ratio. Particle identification or Pid is integrated to the reconstruction in FairShip and distinguishes particles between muons, electrons, and hadrons.

The particle is identified as a muon if it leaves a hit in the first two muon detectors.

If the particle does not hit the muon detectors and has an energy/momentum ratio around 1 the particle is identified as an electron.

If the particle is neither identified as a muon or an electron, it is identified as a hadron.

Based ont the simplicity of this particle identification tool, it is rather obvious that there will still be room for improvement. The first thing to do is to find out how well this Pid tool works on signal and background. The next step is then to see if one can use Pid to increase the signal/background ratio by selecting certain decay modes.

3.8.1 Pid Performance

The first thing to check with Pid is the efficiency of storing information on both fitted tracks of the HNL candidate in signal and background. This efficiency is 99.9 % for HNL signal, while it is around 98 % for the neutrino background.

The next thing to investigate, is to compare the final states identified with Pid to the truth found from the Monte Carlo simulation.
Just like the samples used for the TMVA analysis, the cuts from section 9.2 up to and including the cut on number of degrees of freedom have already been applied.
In tables 21 and 22), the events are shown distributed over particle final states found with Pid on the horisontal axis and with referring to the Monte Carlo simulation on the vertical axis.

One can find the total number of events in a given final state by referring to MCtracks when adding horisontally, while on can find the number of events classified as that particular final state with Pid when adding vertically. The diagonal elements of the tables show the final states that are correctly identified with Pid.

One can see from tables 21 and 22 that there is still room for improvement on the Pid tool, but it should still be possible to use it at the present stage to optimize the signal/background ratio.

MC\Pid	$\mu+\mu$	$e+\mu$	$\pi+\mu$	$\pi+e$	$\pi+\pi$	$e+e$
$\mu+\mu$	234 (0.81/0.91)	0	54 (0.19/0.04)	0	1 (0.00/0.00)	0
$e+\mu$	8 (0.02/0.03)	441 (0.88/0.92)	10 (0.02/0.01)	43 (0.09/0.28)	0	0
$\pi+\mu$	14 (0.01/0.06)	39 (0.03/0.08)	1267 (0.87/0.95)	6 (0.00/0.04)	123 (0.09/0.23)	0
$\pi+e$	0	0	0	86 (0.91/0.55)	1 (0.01/0.00)	6 (0.07/0.06)
$\pi+\pi$	0	0	2 (0.01/0.00)	16 (0.04/0.10)	419 (0.96/0.77)	1 (0.00/0.01)
$e+e$	0	0	0	5 (0.05/0.03)	0	96 (0.94/0.93)

Table 21: HNL signal with 1 GeV mass and all visible decay modes open after the N.d.f cut. The numbers in parenthesis are efficiency/purity

MC\Pid	$\mu+\mu$	$e+\mu$	$\pi+\mu$	$\pi+e$	$\pi+\pi$	$e+e$
$\mu+\mu$	24 (0.21/0.89)	0	79 (0.69/0.21)	0	12 (0.10/0.03)	0
$e+\mu$	0	31 (0.47/0.80)	5 (0.08/0.01)	21 (0.32/0.09)	2 (0.03/0.01)	1 (0.02/0.00)
$\pi+\mu$	3 (0.01/0.11)	8 (0.02/0.21)	300 (0.63/0.78)	10 (0.02/0.04)	156 (0.33/0.36)	0
$\pi+e$	0	0	0	102 (0.77/0.44)	14 (0.11/0.03)	4 (0.03/0.02)
$\pi+\pi$	0	0	1 (0.00/0.00)	36 (0.13/0.16)	242 (0.86/0.56)	1 (0.00/0.00)
$e+e$	0	0	0	64 (0.21/0.28)	6 (0.02/0.01)	229 (0.74/0.97)

Table 22: Neutrino background after the N.d.f cut. The numbers in parenthesis are efficiency/purity

3.8.2 Optimisation using Pid

The optimisation of the signal/background ratio will go as follows: First, find out the cuts to apply, then select final states with a low background rate while suppressing final states with a high background rate.

So starting with the cuts:
The applied cuts are the same used in the tables in section 9.2 with the exception that the momentum is required to be above 1.5 GeV instead of 1 GeV. The cuts used are shown in table 23, and one can see that the increased momentum cut has a signal efficiency of 98 %. In table 24, one can see the neutrino events passing each cut after the N.d.f cut, where the events are distributed over final states.

	Selection	Efficiency	Experiment
Tracks reconstructed	4188		2962
1HNL	3945	94%	2790
Vertex in fiducial volume	3333	84%	2357
Tracks in fiducial volume	3072	92%	2173
N.d.f.>25	2874	94%	2035
DOCA<1 cm	2614	91%	1849
$\chi^2/N.d.f. < 5$	2613	100%	1848
Daughters P>1.5 GeV	2563	98%	1813
IP<250 cm (Ip<10 cm)	2435 (929)	95%	1722
Not Vetoed	2298 (897)	94%	1625

Table 23: HNL decay into visible final states with the same cuts applied as in table 13 with the exception of the momentum cut which has been increased to 1.5 GeV

The way to suppress the final states with many background events is to tighten the cut on impact parameter down to 10 cm instead of 250 cm.

One can make an initial check for each final state if the signal/background ratio increases by selecting it and rejecting everything that is not identified as that given final state. This can be done by comparing tables 25 and 24, where one can use the signal/background ratio at the N.d.f cut for selecting the full signal and full background as reference. This value for signal is found for the

Decay Product	N.d.f > 25	Doca<1 cm	χ^2/N.d.f<5	P > 1.5 GeV	Ip < 250 cm
$\mu + \mu$	27	2	2	2	1
$e + \mu$	39	4	4	2	1
$\pi + \mu$	385	24	24	20	12
$\pi + e$	233	35	35	22	15
$\pi + \pi$	432	62	62	41	21
$e + e$	235	65	65	37	20

Table 24: Neutrino background final states identified with Pid

Decay Product	N.d.f > 25	Ip < 10 cm	Veto	Ip < 250 cm	Veto
$\mu + \mu$	256	23	23	214	213
$e + \mu$	480	31	31	410	408
$\pi + \mu$	1333	754	729	1177	1085
$\pi + e$	156	45	41	107	97
$\pi + \pi$	544	74	71	451	420
$e + e$	103	2	2	76	75

Table 25: HNL final states at 1 GeV according to Pid

Cut	$\mu + \mu$	$e + \mu$	$\pi + \mu$	$\pi + e$	$\pi + \pi$	$e + e$
Fiducial	1730	1157	7125	2752	5809	4114
Veto	4	0	20	0	15	1

Table 26: Neutrino final states passing the veto - and fiducial cuts

simulation in table 23 and the value for background in table 24 where one has to sum a little. The result for the total signal/background ratio is 1.93. Selecting the $\mu + \mu$ final state in tables 24 and 25 increases this ratio to 9.48. One can do the same for the rest of the final states and find that there is a gain in signal/background ratio for the $\pi + \mu$ - and $e + \mu$ final states.

The $\mu+\mu$ - and $e+\mu$ final states are sensitive to the cut on impact parameter as one can see in table 25, where about 10 % of the signal remains after applying the Ip < 10 cm cut. One can see in table 21 that there is some drifting from the $\pi + \mu$ final state in these selections so th real signal with these final states is actually more sensitive to the cut on impact parameter.

Even though the $\pi+\mu$ final state increases the signal/background ratio when selected alone, the efficiency for this final state is 57 % after the 10 cm cut on impact parameter. One thing that one should be aware of is that the $\pi + \mu$ final state also contains the $HNL \to \rho + \mu$ decay, which has a larger impact parameter due to the $\rho^+ \to \pi^+ + \pi^0$ decay. The cut on impact parameter is set to 10 cm for this final state since it is not clear that the signal/background ratio will increase when only selecting the $HNL \to \rho + \mu$ decay.

The rest of the final states require further analysis before a decision can be made on whether or not to suppress them.

One can start by looking at the efficiency for passing the veto cut for each final state, which is what has been done in table 26. The fiducial cut has also been applied to the neutrino background based on the assumption that the distribution of final states passing the veto cut might change under the geometric constraints from the fiducial cuts.

One can see from table 26 that the $e + e$ final state has an efficiency that is ten times smaller than the $\pi + \mu$, $\pi + \pi$ and $\mu + \mu$ final states.

MC\Pid	$\mu+\mu$	$e+\mu$	$\pi+\mu$	$\pi+e$	$\pi+\pi$	$e+e$
$\mu+\mu$	0	0		0	3 (1.00/0.14)	0
$e+\mu$	0	0	0	0	0	0
$\pi+\mu$	1 (0.06/1.00)	1 (0.06/1.00)	11 (0.61/0.92)	0	5 (0.28/0.24)	0
$\pi+e$	0	0	0	15 (0.94/1.00)	0	1 (0.06/0.05)
$\pi+\pi$	0	0	1 (0.07/0.08)	0	13 (0.93/0.62)	0
$e+e$	0	0	0	0	0	19 (1.00/0.95)

Table 27: Neutrino background after cutting on all variables up to and including Ip$<$250 cm. The numbers in parenthesis are efficiency/purity

One also finds the $\pi+e$ final state to have zero efficiency. One can also see from table 27 that both the $\pi+e$ - and the $e+e$ final states have a high purity. This means that one does not have to suppress the $\pi+e$ - and $e+e$ final states.
The only problem with the $\pi+e$ - and $e+e$ final states is that the signal yield is very small for both of them at an HNL mass of 1 GeV.
A final argument for keeping the $e+e$ final state is that this analysis has been done assuming normal neutrino mass hierarchy, while it is just as likely that the neutrino mass hierarchy is inverted. For inverted neutrino mass hierarchy the mixing parameter U_e^2 can be much higher than U_μ^2 [8].

The $\pi+\pi$ final state has the highest background level, but also geves a significant contribution to the signal. Two models are therefore made, one keeping the $\pi+\pi$ final state, and one suppressing it.

What remains to figure out is the expected background level after the veto cut. From section 9.2, it was found that the veto efficiency has an upper bound of 1.2%. When including the antineutrino background and scaling the neutrino background to what is expected during the experiment, one ends up with a background of 1.0 event.

In table 28 one can find the result of this analysis with the selected final states, the signal and the background.

Since the results are based on a rather simple particle identification tool, improvements might change the resulting background level a bit.

Label	Ip<250 cm	Ip<10 cm	Signal	Background
Ip<250 cm	all	none	2298	1.0
Pid 1	$e+e$	$\pi+\mu$	1942	0.66
	$e+\mu$			
	$\mu+\mu$			
	$\pi+\pi$			
	$\pi+e$			
Pid 2	$e+e$	$\pi+\mu$	1593	0.104
	$e+\mu$	$\pi+\pi$		
	$\mu+\mu$			
	$\pi+e$			
Ip<10 cm	none	all	897	< 0.012

Table 28: Result from selections with Pid

3.9 SHiP Sensitivity Range

The goal for the SHiP experiment along with all other experiments of this scale is to explore regions of certain parameters that have not been reached before, and in the HNL case, this is the mixing to the Standard Model, U^2 that can extend down to the region where the νMSM can be verified. In order to cover as much of this region, one has to be able to determine the exeistence of HNLs with as few detected HNL candidates as possible.

The goal in this section is to find the sensitivity range for detecting HNLs with SHiP when the cuts found in the optimisation with Pid are applied.
2 HNL candidates will be enough do determine the existence of HNLs with 99 % certainty when the background is 0.1 or below. In order to get 2 events with 90 % certainty one has to expect around 6 HNL events, since 90 % of the events lie within 1.6 σ of the expected value and with the assumtion of a Poisson distribution 6 events have $\sigma \approx \sqrt{6}$. If the background is higher than this, the detected number of HNL candidates should scale as:

$$N_{HNL} \geq N_{bg} + 3\sigma_{bg}, \tag{19}$$

where N_{HNL} is the number of detected HNLs and N_{bg} is the number of background events.

The results from eq. 19 are shown in table 29 for background levels within the estimated range found in the analysis.

With this information, one can find the sensitivity range for the 1 GeV HNL with the different optimisations used.

The next step is to extend the sensitivity range to cover the whole mass spectrum of interest in SHiP. In order to do that, one has to make some assumptions where the most important one is that the cut efficiency for each HNL final state is invariant over mass.
One can then find out how the branching ratio of each HNL final state evolves over HNL mass. This is shown in fig. 24 for the HNL decay modes included in

N_{bg}	N_{HNL}
(0, 0.005)	1
(0.005, 0.1)	2
(0.1, 0.33)	3
(0.33, 0.67)	4
(0.67, 1.1)	5

Table 29: Intervals for background level with the required signal to be 3σ away from background

the simulations.

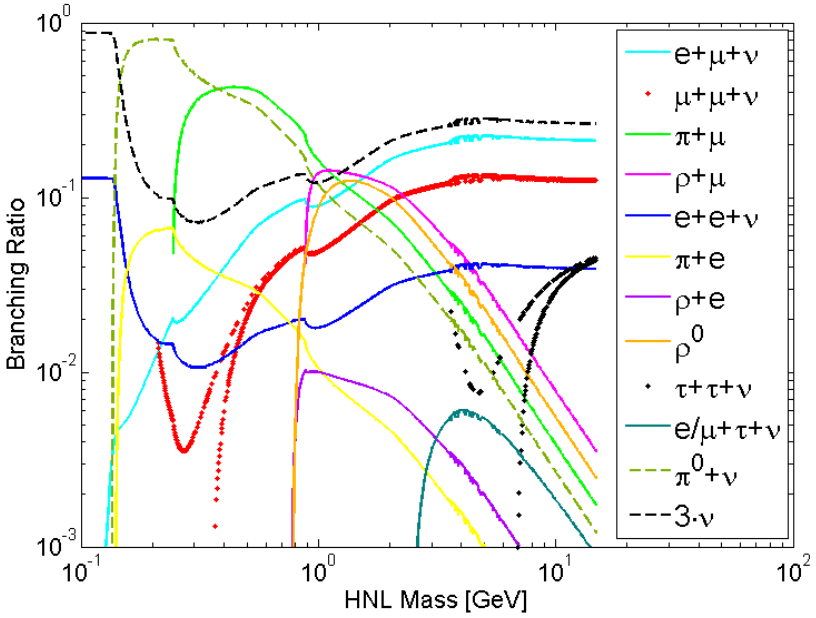

Figure 24: Branching ratios for the HNL decay modes that are included in FairShip so far as a function of HNL mass with $U^2 = (4.47 \cdot 10^{-10}, 7.15 \cdot 10^{-9}, 1.88 \cdot 10^{-9})$ the dashed lines represent invisible decay modes, while dots show oscillating decay modes. Other decay modes have also been part of the computation of the branching ratios.

There are also other HNL decay modes that are only used to compute the HNL decay rate, but some of these decay modes heve some detectable final states. The branching ratios for the decay modes not included in the simulations are shown in fig. 25.

The branching ratios from the HNL decay modes can then be used togeter with the reconstruction - and cut efficiencies of each HNL decay mode to find the total HNL efficiency at a given mass.

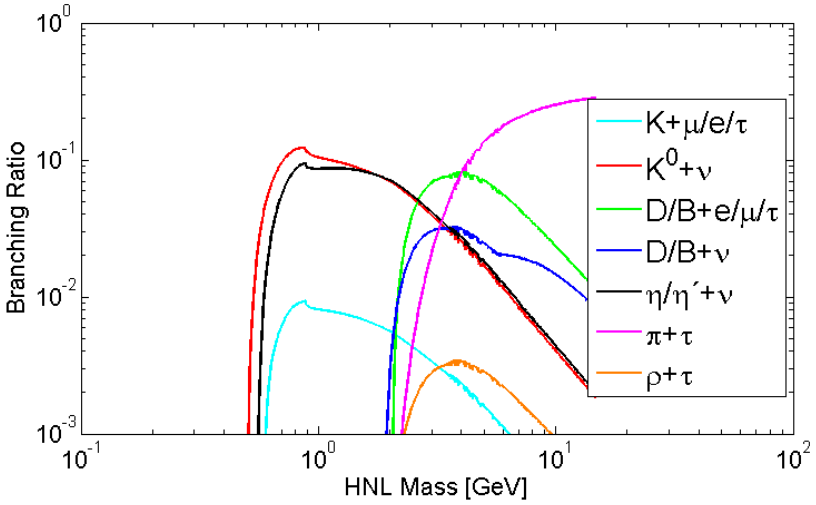

Figure 25: Branching ratios for the HNL decay modes that are not included in FairShip so far as a function of HNL mass with $U^2 = (4.47 \cdot 10^{-10}, 7.15 \cdot 10^{-9}, 1.88 \cdot 10^{-9})$.

The resulting efficiencies are shown in fig. 26.

The data from fig. 26 along with information on the background can then

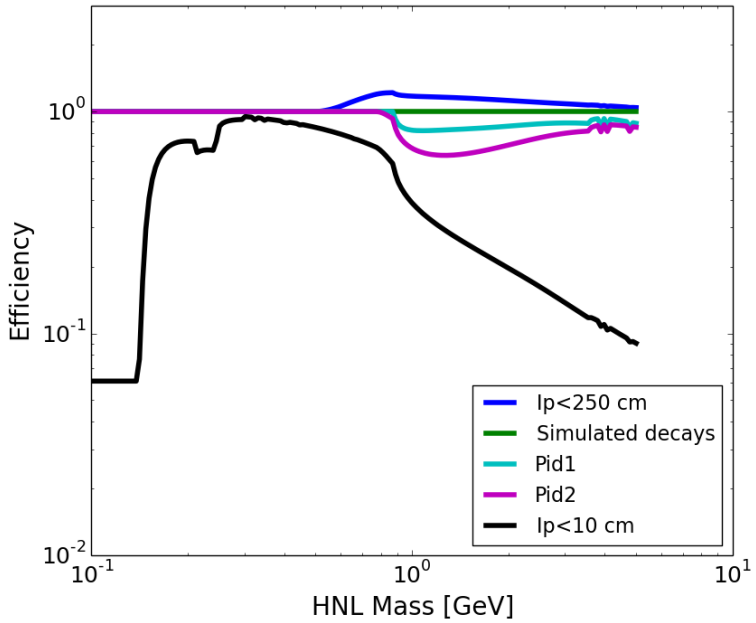

Figure 26: Signal efficiencies for different cuts based on branching ratio

be used to adjust the sensitivity range for the SHiP experiment. Since the

simulations behind the sensitivity plot include the same HNL decay modes as FairShip, it is in principle based on the branching ratio for the simulated events, the adjustments will follow the equation below:

$$U^2 \propto \sqrt{\frac{\text{Eff}_{sim}}{\text{Eff}_{cut}}} \cdot \sqrt{\frac{N_{HNL}^{90\%}}{N_{0.1}^{90\%}}} \tag{20}$$

Where Eff_{sim} is efficiency for the generation of visible simulated events, while Eff_{cut} is the efficiency for generating the final states that are not suppressed by the cuts and 2 % of the suppressed final states. $N_{HNL}^{90\%}$ is the number of HNL events required for the 90 % lower bound to be three sigma away from the background, while $N_{0.1}^{90\%}$ is the 90 % confidence level to get 2 HNL events in order to be 3σ away from a background of 0.1.

What remains to be done is to apply the efficiencies found to the SHiP sensitivity range over the whole mass spectrum, scaled to match the result from the estimated HNL yield after all cuts are applied.
The data used for the ShiP sensitivity over the relevant mass spectrum, was borrowed from the SHiP Collaboration.
The cuts applied in the Toy MC are different from the cuts applied to HNL signal in this report, but it has been used in any case and scaled according to the applied cuts.

After all cuts from table 23 are applied, with Ip $<$ 250 cm selected, there will be 1625 HNL events remaining at $U^2 = 9.5 \cdot 10^{-9}$ and 1 GeV mass with an expected background of 1 event. This means that one can expect a lower limit at $U^2 = 7.52 \cdot 10^{-10}$
The result from the scalings of the SHiP sensitivity to match the applied cuts is shown in fig. 27. The boundaries shown in fig. 27, are the boundaries for the νMSM, as mentioned in section 1.4.

As seen in fig. 27, most of the cuts from the optimisation with Pid do not make that much difference in the SHiP sensitivity range, except for the Ip $<$ 10 cm cut on all final states which significantly decreases the sensitivity range in the mass region around 2 GeV. In the mass region of 0.3 to 0.5, the signal is rather robust to the cuts applied, even the cut on Ip $<$ 10 cm on everything.

The optimal solution changes at an HNL mass around 0.8 GeV, where the most efficient cuts at the lower masses will be the least efficient at higher masses. This means that one either has to work with two sets of cuts, or one could choose a compromise, which in this case is one of the selections with Pid.

For comparison, the SHiP sensitivity range at 1 GeV published in [8] has the value; $U^2 = 7.6 \cdot 10^{-10}$ for normal hierarchy, which is very close to the results from my applied cuts. These sensitivities are based on completely different approaches to select the HNL signal, and the background level has been set to 0.1 without a direct implementation of cuts to justify this backround level.
My studies have at least shown that the SHiP sensitivity range given in [8] can be reached when applying a smart selection of cuts.

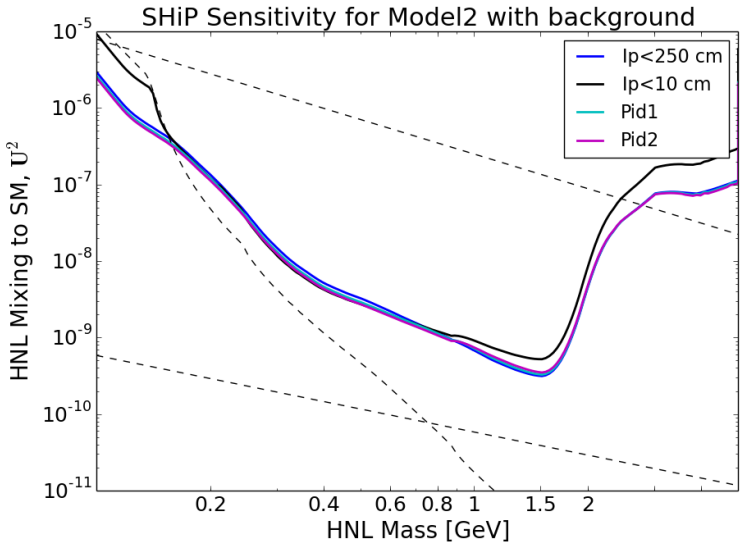

Figure 27: SHiP sensitivity with background taken into account.

Conclusion

In this report, I have estimated the signal yield of HNLs at a chosen mass and mixing parameter that are within the bounds of the νMSM.
I explored the use of cuts and methods of multivariate analysis, and found that using cuts performed better than the multivariate methods used in this analysis. One could try tofind ways to decorrelate the variables used in the multivariate analysis.
The cuts were optimised for HNL signal with a mass of 1 GeV, and it was found that the optimal cuts either had a high momentum requirement or a strong requirement on impact parameter.

I have used particle identification to optimize the sensitivity range for finding HNLs in SHiP, and made an estimate on this sensitivity range.
One study that will be interesting with regards to particle identification is to seperate the $\pi + \mu$ and $\rho + \mu$ final states to optimize these cuts further.
Since the original design of the SHiP experiment [8], many studies have been made with regards to optimising the performance and reliability of the experiment.
These studies have lead to some changes in the design of the experiment, especially one consideration is interesting which is to replace the vacuum vessel with a helium balloon.
Under these conditions, particle identification studies will be necessary to keep the background at an acceptable level.

References

References

[1] Ship Collaboration home page: http://ship.web.cern.ch/ship/

[2] S.F. Novaes, *"Standard Model: An Introduction"*, IFT-P.010/2000, arXiv:hep-ph/0001283.

[3] L. Canetti, M. Drewes, T. Fossard, M. Shaposhnikov, *"Dark Matter, Baryogenesis and Neutrino Oscillations from Right Handed Neutrinos"*, Phys. Rev. D 87, 093006 (2013), [arXiv:1208.4607].

[4] R. D. Klauber, *"Student Friendly Quantum Field Theory: Basic Principles in Quantum Electrodynamics"*, Sandtrove Press, 2013, ISBN 9780984513932

[5] The SHiP Collaboration, *"A facility to Search for Hidden Particles at the CERN SPS: the SHiP physics case"*, CERN-SPSC-2015-017 / SPSC-P-350-ADD-1 08/04/2015

[6] K.A. Olive et al. (Particle Data Group), Chin. Phys. C, 38, 090001 (2014) and 2015 update

[7] J.J. Gomez-Cadenas, J. Martin-Albo , M. Mezzetto, F. Monrabal, M. Sorel, *"The Search for neutrinoless double beta decay"*, Riv.Nuovo Cim. 35 (2012) 29-98,arXiv:1109.5515 [hep-ex].

[8] The SHiP Collaboration, *"Technical Proposal, A Facility to Search for Hidden Particles (SHiP) at the CERN SPS"*, CERN-SPSC-2015-016 / SPSC-P-350 08/04/2015

[9] B. Kayser, *"Are Neutrinos Their Own Antiparticles?"*, FERMILAB-CONF-09-058-T, [arXiv:0903.0899].

[10] O. Ruchayskyi and A. Ivashko, *"Experimental bounds on sterile neutrino mixing angles"*, JHEP1206(2012) 100, [arXiv:1112.3319].

[11] Planck Collaboration, P. Ade et al., *"Planck 2013 results. XVI. Cosmological parameters"*,Astron.Astrophys. (2014) [arXiv:1303.5076].

[12] M. Shaposhnikov, *"A possible symmetry of the νMSM"*, Nucl. Phys. B763 (2007) 49ï¿½59 [arXiv:hep-ph/0605047].

[13] D. Gorbunov, I Timiryasov, *"Testing νMSM with indirect searches"*, Phys. Lett. B 745, 29 (2015), arXiv:1412.7751v2 [hep-ph].

[14] http://home.cern/about

[15] The SHiP Collaboration, *"Addendum to Technical Proposal, A Facility to Search for Hidden Particles (SHiP) at the CERN SPS"*, CERN-SPSC-2015-040 / SPSC-P-350-ADD-2 19/10/2015

[16] P. Hansen, *"Particle detectors and accelerators, Lecture notes"*, Polyteknisk Forlag, 2015 First edition.

[17] https://github.com/ShipSoft/FairShip

[18] D.P.Landau, K. Binder, *A Guide to Monte Carlo Simulations in Statistical Physics*, Cambridge University Press, 2014 Fourth Edition, ISBN 1107074029

[19] T. Sjostrand, S. Mrenna, and P. Skands, *"A brief introduction to PYTHIA 8.1"*, Com- put.Phys.Commun. 178, 852-867, (2008). doi: 10.1016/j.cpc.2008.01.036.

[20] S. Agostinelli et al., *"GEANT4: A Simulation toolkit"*, Nucl.Instrum.Meth. A506, 250-303, (2003). doi: 10.1016/S0168-9002(03)01368-8.

[21] C. Andreopoulos, A. Bell, D. Bhattacharya, F. Cavanna, J. Dobson, et al., *"The GENIE Neutrino Monte Carlo Generator"*, Nucl.Instrum.Meth. A614, 87-104, (2010). doi: 10. 1016/j.nima.2009.12.009.

[22] A. Hoecker, P. Speckmeyer, J.Stelzer, J.Therhaag, E. Von Toerne, H. Voss *"TMVA4 Toolkit for Multivariate Data Analysis with ROOT Users Guide"*, arXiv:physics/0703039[Data Analysis, Statistics and Probability], CERN-OPEN-2007-007, TMVA version 4.2.0, October 4, 2013; http://tmva.sourceforge.net/docu/TMVAUsersGuide.pdf

[23] https://root.cern.ch/about-root

[24] D. Gorbunov and M. Shaposhnikov, *"How to find Neutral Leptons of the νMSM?*, JHEP. 0710, 015, (2007). doi: 10.1007/JHEP11(2013) 101,10.1088/1126-6708/2007/10/015.

Appendix

$$\mathcal{L} = \mathcal{L}_{\mathrm{SM}} + i\bar{N}_I\gamma^\mu\partial_\mu N_I - \left(F_{\alpha I}\bar{L}_\alpha N_I\tilde{\Phi} + \frac{M_{I,J}}{2}\bar{N}_J^C N_I + h.c.\right)\text{[10]}, \qquad (21)$$

In this Lagrangian, the term "$i\bar{N}_I\gamma^\mu\partial_\mu N_I$" is the kinetic energy term for the right handed neutrino.

N is an operator that destroys a right handed neutrino field and creates a charge conjugated field, while $\bar{N} = CN^T\gamma^0$ where γ^0 is an identity matrix with the sign reversed in the lower half, C is a charge conjugation, and N^T is the transpose of the N operator. This means that $\bar{N}^c = \gamma^0 N^T$. Hermitian conjugation is the transformation: $\bar{N} \leftrightarrow N$.

The same rules apply to L and the term $F_{\alpha I}\bar{L}_\alpha N_I\tilde{\Phi}$, where the only nonzero contribution of the lepton doublet is the left handed neutrino field due to the vev of the Higgs doublet. This means that since N creates a right handed antineutrino, which is the charge conjugate of a left handed neutrino, the term $\bar{L}N$ creates a left handed neutrino from a right handed neutrino.

The term $F_{\alpha I}\bar{L}_\alpha N_I\tilde{\Phi}$ is similar to the Higgs coupling to the other fermions that are Dirac particles and is therefore called a Dirac mass term.

The term $\frac{M_{I,J}}{2}\bar{N}_J^C N_I$ creates two charge conjugates of the right handed neutrinos from two right handed neutrinos.

The hermitian conjugates are the reversed processes.